Al-Mukhtar Journal of Basic Sciences

Volume 22 | Issue 2 AUG 2024

EISSN:3006-8649

Published by OMU

Al-Mukhtar Journal of Basic Sciences

Peer-reviewed scientific journal, Volume Twenty-Two, Issue Two, 2024

Published by Omar Al-Mukhtar University, Al-Bayda, Libya

A peer-reviewed journal published by Omar Al-Mukhtar University,

Al Bayda, Libya

Peer-reviewed scientific journal, Volume Twenty-Two, Issue Two, 2024

Email: ljbs.sci@omu.edu.ly

EDITORS & STAFF

Al-Mukhtar Journal of Basic Sciences 22: (2), 2024

Al-Mukhtar Journal of Basic Sciences 22 (2): 103-113, 2024
Doi: https://doi.org/10.54172/0xd07091

Research Article **Open Access**

Comparison between Green and Chemical Synthesis of Silver Nanoparticles: Characterization and Antibacterial Activit

Dalal M Ibrahim[1*], Hamad M Idris[2] and Hind M Mohammed[3]

***Corresponding author:** dalal.m.ibrahimple@omu.edu.ly
Department of Chemistry, Omar Al-Mukhtar University, Libya.

[2] Department of chemistry, Omar Al-Mukhtar University, Libya.

[3] Department of Chemistry, Libyan Academy, Al-Jabal Al-Akhdar Branch.

Received:
14 April 2024

Accepted:
26 June 2024

Publish online:
31 August 2024

Abstract
Using chemical reduction and green technology, two different approaches are used in the current work to synthesize silver nanoparticles. Pomegranate peel extract has been utilized in green technology applications. Furthermore, In the chemical approach, polyvinylpyrrolidine and ascorbic acid were utilized as reducing agents, and the optical, structural, and antibacterial characteristics of the two versions were investigated. In comparison to the chemical reduction variant (30.38 nm), the particle sizes in the green technique (19.5 nm) were smaller. Comparing green silver nanoparticles to chemically synthesized silver nanoparticles, SEM pictures showed that the former had formed a distinct crystalline shape and were evenly distributed on the surface. Granules constituted the shape of the particles. Additionally, it spreads topically. Whereas the greenly synthesized variant's absorption band was at 280 nm, the chemically synthesized variant's absorption band was at 300 nm. It was demonstrated by spectroscopic data of green silver nanoparticles that they have the capacity to produce and stabilize silver nanoparticles. Chemically produced green silver nanoparticles were also exposed to FTIR analysis to identify active functional groups. Silver particles can also be stabilized by chemically produced silver nanoparticles. To assess the antibacterial activity, the nanoparticle agar diffusion method was employed. The bacteria detected in the medium were Staphylococcus aureus and Escherichia coli. In the green form, the bacterial growth inhibition zone was larger and was produced with varying concentrations of 25 ml, 50 ml, 75 ml, and 100 ml, or 13 ml, 10 ml, 9 ml, and 8 ml for Staphylococcus aureus and 15 ml, 12 ml, 10 ml, and 7 ml for E. coli, respectively. Green-produced transcripts exhibited higher antibacterial responses, which were likely caused by the faster rate of nanoparticle stabilization mechanism by organic compounds found in pomegranate fruit peel extract.

Keywords: Nanoparticles, Green Method, Chemical Method, Antibacterial Activity, silver Nanoparticles

INTRODUCTION

Civilization has been gradually shifting towards more environmentally friendly and sustainable methods in all areas of growth during the 20th century, sometimes known as the post-industrial era (Venhoeven, Bolderdijk, & Steg, 2016). Searching for new, more environmentally friendly and sustainable ways to do the things we do every day. Difficulties that require immediate attention include

resource depletion, climate and ecosystem changes, insufficient access to drinking water, poor air quality, and other major problems (Ibrahim, Abdelghani, Anwagy, & Rizkallah, 2024; Venhoeven et al., 2016).Consumption is particularly high in the construction industry, where the life cycles of building materials consume a large amount of energy (Küünal, Kutti, Rauwel, Guha, et al., 2016; Küünal, Kutti, Rauwel, Wragg, et al., 2016).

The years have seen a shift in focus towards green and smart housing. Use natural, affordable and environmentally friendly building materials The basic concept of green housing, and the choice of environmentally friendly options depends largely on the quality of the Indoor climate. Research organizations have studied nanomaterials in great detail over the past 20 years. Providing special qualities and methods to make our daily lives better (Huang, Liu, & Wang, 2020;Jadoun, Verma, & Arif, 2020). Metal nanoparticles are very promising in creating new antibacterial agents (Rai, Ingle, Birla, Yadav, & Santos, 2016). Synthesis techniques, which are the traditional methods used to create metallic silver nanoparticles, are usually uneconomical. In certain situations, they also require harmful reagents, along with specialized tools and knowledge. In addition, many of the synthesis procedures are typically energy-intensive and lead to the production of toxic byproducts (Küünal, Rauwel, & Rauwel, 2018). Thus, It is necessary to create technologies that are economical and environmentally appropriate, and biosynthetic technologies appear to offer the greatest promise in this regard (Rauwel, Küünal, Ferdov, & Rauwel, 2015).

Because they offer straightforward methods and a variety of plant material options. Nanomaterials are materials with length scales of 1–100 nm in at least one dimension. The synthesis of nanoparticles as an emerging feature of the convergence of nanotechnology and biotechnology has attracted increasing interest due to a growing desire to be environmentally benign. Nanoparticles are particularly promising for development because they exhibit antibacterial capabilities due to their enormous surface area and volume ratio. The current topic has become under study due to the Increasing resistance of microbes to metal ions and the emergence of resistant strains (Fayaz et al., 2010). For these reasons, silver has long been known to be harmful to 116 different microorganisms (Liau, Read, Pugh, Furr, & Russell, 1997) and Is widely used in bactericidal applications (Gupta & Silver, 1998; Nomiya et al., 2004). The bactericidal effect of silver Ions on microorganisms is well known. Their derivatives are commercially exploited as antibacterial agents. Understanding of the bactericidal mechanism is still limited. A strong interaction with the thiol groups of essential enzymes, leading to their inactivation has been proposed (Gupta & Silver, 1998). Based on experimental results, DNA replication is inhibited once bacteria are exposed to silver ions Studies conducted by (Singh, Singh, Prasad, & Gambhir, 2008). demonstrated the presence of small electron-dense granules generated from sulfur and silver, along with structural changes in the cell membrane. Compared to both bulk materials and ions, metal particles with sizes In the nanometer range have distinct physical properties.

Their architecture with highly active facets makes them display exceptional features such as enhanced catalytic activity (Singh et al., 2008).Thanks to their ability to reduce metal ions, microorganisms including fungi and bacteria are now an important part of the toxic metal remediation process (Kalishwaralal, Deepak, Ramkumarpandian, Nellaiah, & Sangiliyandi, 2008).

MATERIALS AND METHODS

Green Method for Preparing Silver Nanoparticles

The type of plant used in this study, which is pomegranate fruit, has been identified, and the peels will be used In this experiment. And cover the AGNPs so that they are more beneficial to humanity. The pomegranate peels were extracted with a solvent, which is distilled water. To determine the

best nano-result, the pomegranate peels were air-dried for two weeks and then crushed using a mortar and pestle. 8 g of powder was weighed using a weighing scale and placed in a 250 ml beaker, and 200 ml of solvent (distilled water) was added to the beaker. The mixture was heated for 30 min using a water bath and then filtered through filter paper and then stored in the refrigerator for further use. An aqueous solution of silver nitrate was prepared to synthesize AgNPs. 50 ml of pomegranate extract solution was added to 5 ml of silver nitrate with stirring to reduce the Ag ions to the collected silver groups and then the solution was left for 24 hours until sedimentation to obtain silver nanoparticles.

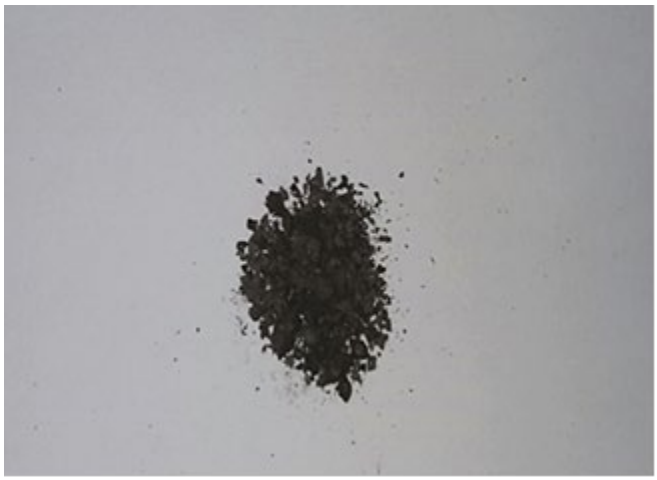

Figure: (1). Green Silver Nanoparticles

Chemical Method for Preparing Silver Nanoparticles

First, a silver nitrate solution was prepared by adding 4g of AgNO3 to 40ml of distilled water and then 20ml of ascorbic acid, solution (A), was added. A PVP solution was prepared by dissolving PVP and glucose in 60 ml of distilled water together, yielding solution (B). Solution B is then heated to a temperature of 60°C by a magnetic stirrer. After stabilizing the temperature for (15 minutes), solution (A) Is added to (B) dropwise. Then the mixed solution was stirred for (10 – 15 minutes) and a brown powder was formed. Then it was dried for 30 minutes at 100 degrees Celsius. Finally, 50 ml of sodium hydroxide (NaOH) was gradually added to the solution until the pH turned to 11.

Figure: (2). Chemically Manufactured Nanoparticles Silver

Antimicrobial Action

Bacterial cultures: nutrient medium agar farms were used to grow bacteria. 850 milliliters of sterilized distilled water were used to dissolve 14 grams of powder to create the medium. After 15

minutes of sterilization at 121 °C to disinfect the medium, bacteria were developed and incubated for 24 hours in the incubation at 37 ° C. Antibacterial Assay: Green and Chemical Synthesis and Antibacterial Activity Using the Agar Disc Spreading Method 72 hours in solid cultural media.

RESULT AND DISCUSSION

Physical properties

Table:(1). Some physical properties of green and chemical nanoparticles

Solubility in DMSO	Solubility in etha-nol	Solubility in water	Colour and texture	Average particle size	Size range	Boiling point	Melting point	Nanoparticles	Solubility in HNO3
Highly soluble	Good solvent	Melt with vigorous stirring	Completely soluble	Brown	<100	100_80	2162	961.78	Green silver nanoparticles
Highly soluble	Good solvent	Melt	Completely soluble	Black	<100	80_100	2162	961.78	Chemical silver nano-particles

Scanning Electron Microscopy

The shape of the particles was confirmed by SEM examination. With a working distance (D) of 10.6 mm and a high voltage of 20.0 kV, they were performed at a scale of 200 μm. We show that the silver nanoparticles are well dispersed and have a crystalline morphology, according to the SEM data in Figure 1, while the chemically synthesized silver nanoparticles were synthesized on the 500 μm scale at a high voltage of 20.0 kV and a working distance (D) of 10.1 mm. In this result, the particles are In the form of small grains that are well dispersed, and the aggregation of particles can be seen according to the SEM data in figure 3.

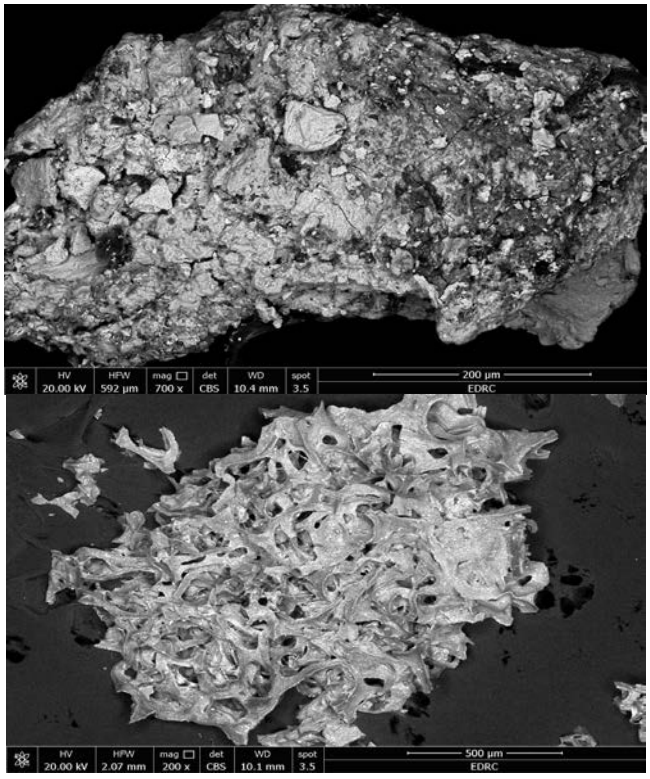

Figure: (3). SEM Micrograph Green Silver Nanoparticles and Chemically Synthesized Silver Nanoparticles

Ultra Violet-Visible Spectroscopy

In the case of the green synthesis method, 30 ml of sample is taken and diluted in 5 ml of distilled water. After half an hour, spectroscopic analysis of green silver nanoparticles was performed and Figure 4 shows the absorption peak at 280 nm and absorbance 1.5. The chemical reduction of silver ions was also monitored in the same way as the first sample dilution. UV spectroscopy was performed as shown in Figure 5 and the absorbance peak was 300 nm and absorbance was 0.4, We note that as the wavelength increases, the absorption intensity decreases, which indicates that the formation did not occur at a large wavelength, so the best formation is for green silver nanoparticles

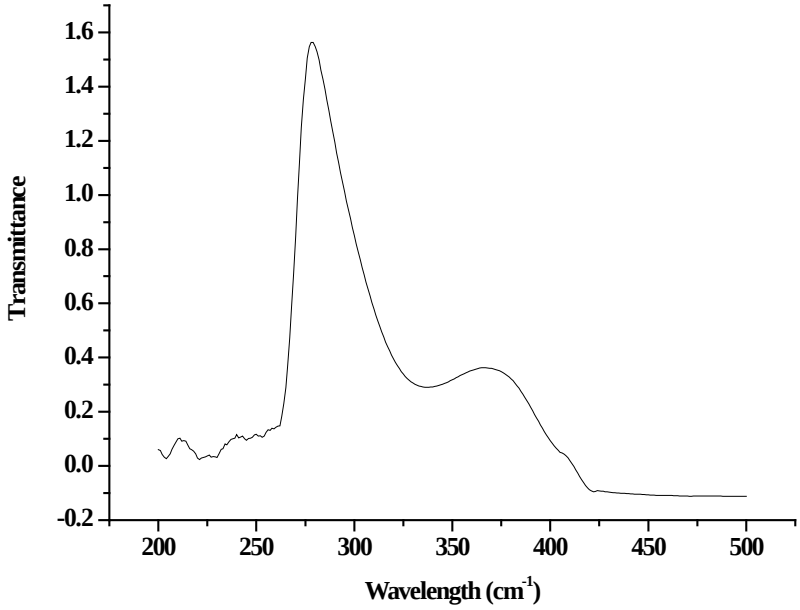

Figure: (4). UV_VIS Spectroscopy of Green Silver Nanoparticles

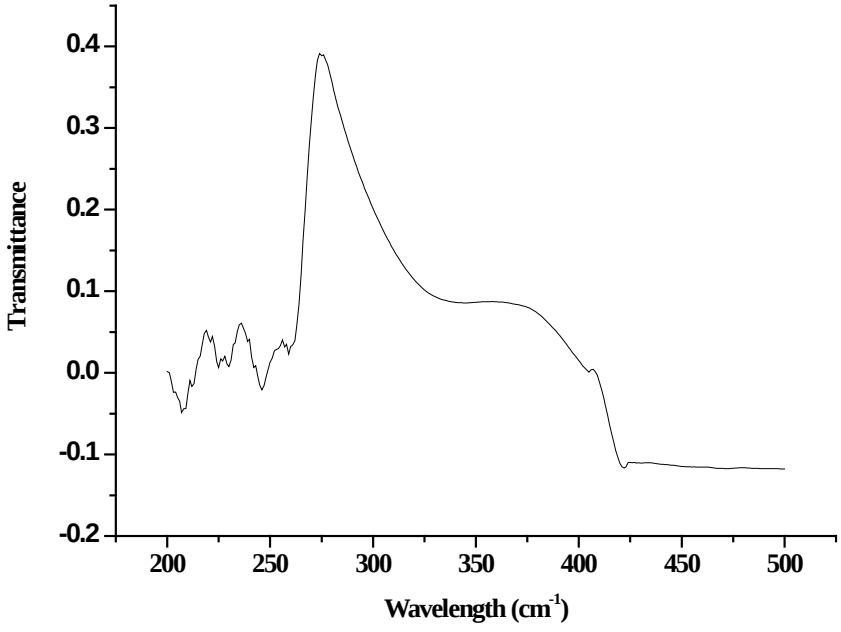

Figure: (5). UV_VIS Spectroscopy of Chemical Silver Nanoparticles

X-Ray Diffraction Analysis

Figure 6 displays the XRD patterns of silver nanoparticles made from pomegranate peel extract. higher proportion of crystalline phases is indicated by the greener peak value displayed by the green nanotube particles. On the contrary, the Debbie-Scherer equation was used to ascertain the crystal size.

$$\text{Particle Size (D)} = K\lambda / (\beta \cos \theta)$$

In this case, μ is the radiation wavelength, θ is the Bragg angle, and K is the dimensionless shape factor 0.94 β represents the full width of the corresponding peak at half maximum as well. D Is essentially the fundamental size of the ordered domains, which is thought to be equivalent to the particle size only relevant to particles smaller than 100. The particle size of green silver nanoparticles can be calculated using the values in the diffraction pattern as follows.

The size of the green nanoparticles produced by the X-ray diffraction pattern was determined:

$$D=K\lambda/(\beta \cos\theta)$$
$$D1=(0.94\times1.54)/(0.184 \cos30.09)$$
$$D=31.12\text{nm}$$
$$D2=(0.94\times1.54)/(0.231 \cos68.43)$$
$$D=7.88\text{nm}$$
$$\text{Average crystallite size= } 31.12+7.88/2$$
$$ACS=19.5\text{nm}$$

The size of the green silver nanoparticles ranges between 31.12nm and 7.88nm, so the average crystallite size is 19.5nm.

By the values in the X-ray diffraction pattern of chemically manufactured nanoparticles we can calculate it as follows

$$D=K\lambda/(\beta \cos\theta)$$
$$D1=(0.94\times1.54)/(0.1332 \cos20.22)$$
$$D=53.20\text{nm}$$
$$D2=(0.94\times1.54)/(0.2008 \cos19.23)$$
$$D=7.56\text{nm}$$
$$\text{Average crystallite size=53.20+7.56/2 } ACS=30.38$$
$$ACS=30.38$$

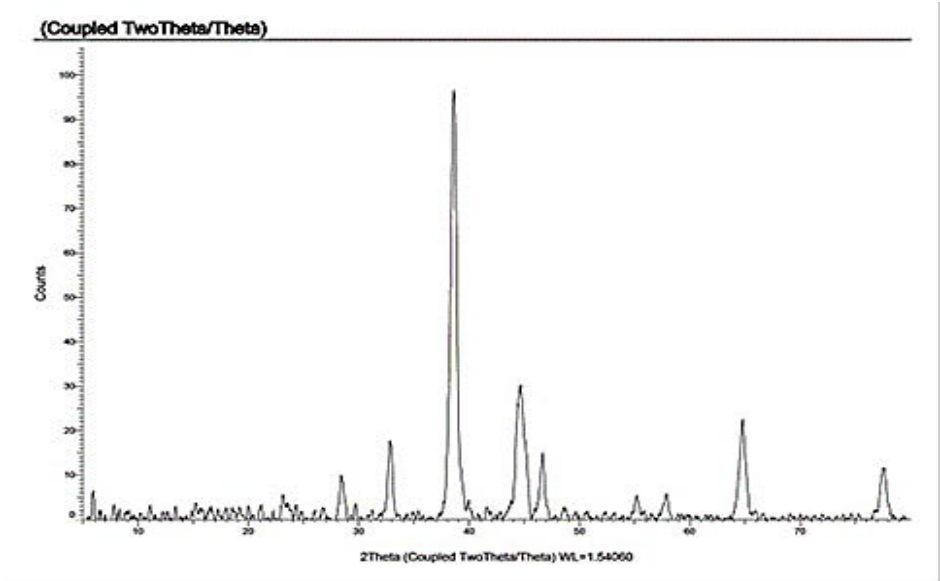

Figure: (6). XRD Diffraction Pattern for Green Silver Nanoparticles

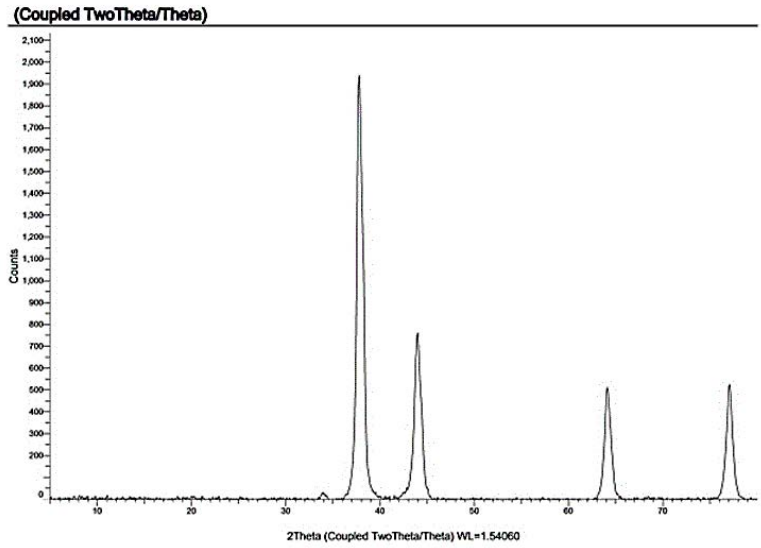

Figure: (7). XRD Diffraction Pattern for Chemically Composite Nano Silver Particle

FTIR Spectroscopy

In order to Identify active functional groups, FTIR is a valuable approach. Figure 8 shows the FTIR spectra of green silver nanoparticles and consists of several bands measured at 2948 cm, 2183.05 cm, 2042.68 cm, 1916.22 cm, 1595 cm, 1392 cm, 858.63 cm, 677.48 cm, 553.09 cm, 498.55 cm. 440.36 cm, Stretching of the hydroxyl molecule is responsible for the band at 29,481 cm, while the aromatic nitro and alkyl vibration modes are responsible for the peak at 1,595.681 cm. The major alcohol in bending or vibration Is responsible for the peak observed at 1392 cm; Either the bands (677.48 cm, 553.09 cm, 498.55 cm, 440.36 cm) are extended for alkyl halides. Evidence suggests that biological molecules may have a role in the stabilization and production of silver nanoparticles: the FTIR spectrum of chemical nanoparticles is shown in Figure 8, which includes multiple bands : 3362.13 cm, 2927.36 cm and 2340.41 cm; 2155.40 cm; 2019 25cm, 1719.95cm, 1643.02cm, 1366.59cm, 1240.31cm; 1021.03 cm; 499.55 cm, the OH (alcohol) or N-H (Ameen) stretches are responsible for the band at 3362.13 cm, while the C-H (alkane) stretch is responsible for the band at 2927.36 cm, while the carbonyl bond group (O=C=O) Is responsible for The range is at 2340.41 cm. The band's N-H (amine) curve appears at 1643.02 cm, while the peak at 1719.95 cm Is the C=O stretch. The secondary alcohol in bending or vibration is responsible for the peak at 1366.59 cm. Based on these facts, we may conclude that chemically synthesized nanoparticles can also contribute to the synthesis and stabilization of nanoparticles.

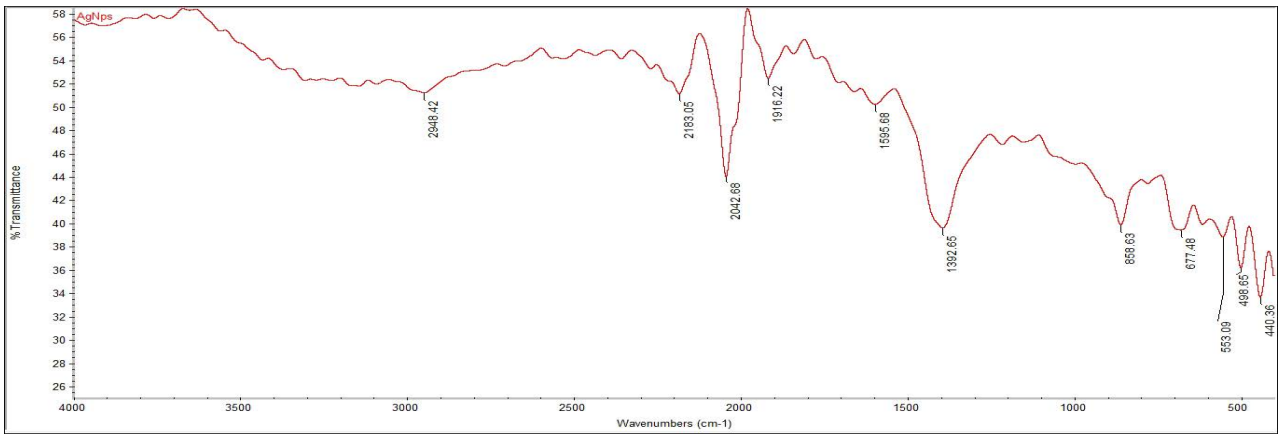

Figure: (8). FTIR Spectra of Green Silver Nanoparticles

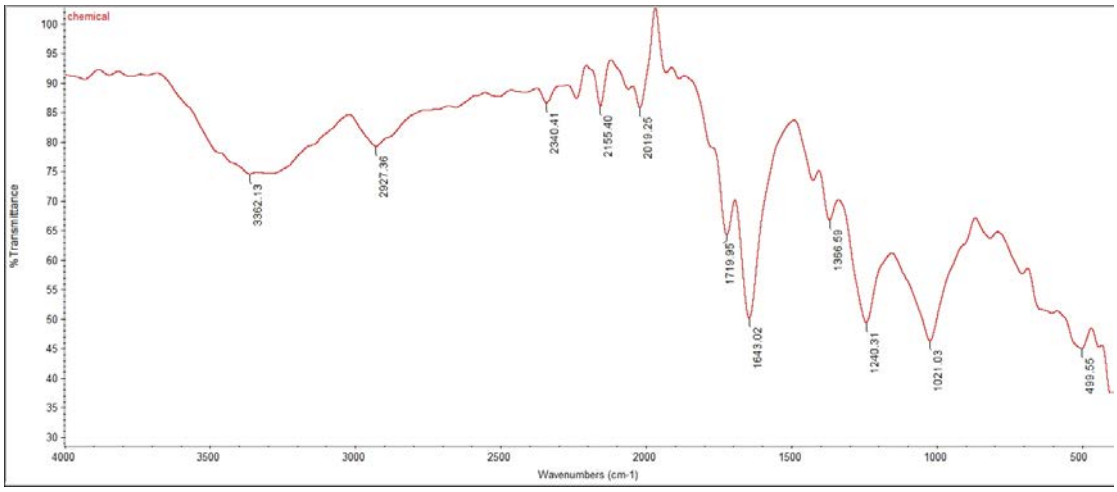

Figure: (9). FTIR Spectra of chemical silver nanoparticles

Antibacterial activity

The antibacterial activity was tested against two distinct strains of bacteria. Green and chemical silver nanoparticles have antibacterial properties against both Gram-positive (Staphylococcus aureus) and Gram-negative (Escherichia coli) pathogens The products were employed in solution form at doses of 25, 50, 75, and 100 mg using the agar diffusion method. After applying all concentrations to the surface of the culture dishes, they were incubated for an entire day at 37°C with the lid on. Following the identification of the compounds' inhibitory effects, it was discovered that the domains of bacterial growth inhibition generated by chemical and green silver nanoparticles were distinct from one another. The ability of nanoparticles to inhibit bacteria is a size-dependent characteristic that gets better as the particle size gets smaller; yet, Compared to chemical silver nanoparticles, green silver nanoparticles exhibit a larger zone of inhibition .and Tables 2 and 3 contain tabular data for the Inhibition zone measurements. Because they have larger surface areas and smaller particle sizes than chemical silver nanoparticles, green silver nanoparticles have greater antibacterial potential.

Table:(1). Antibacterial measurements of green nanoparticles

Sample	Bacteria	Weight of the sample	Bacteria type	Zone inhibition
Green Silver Nanoparticles	Staphylococcus Aureus	25	Gram positive	13
		50		10
		75		9
		100		8
	Escherichia Coli	25	Gram negative	15
		50		12
		75		10
		100		7

Table:(3). Antibacterial measurements of chemical nanoparticles

Sample	Bacteria	Weight of the sample	Bacteria type	Zone inhibition
Green Silver Nanoparticles	Staphylococcus Aureus	25	Gram positive	10
		50		9
		75		9
		100		6
	Escherichia Coli	25	Gram negative	12
		50		10
		75		8
		100		6

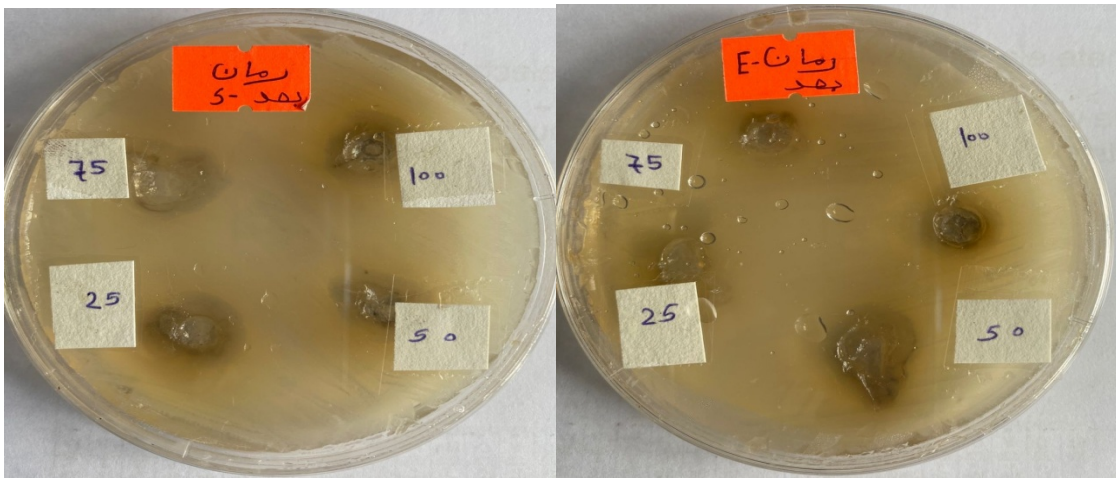

Figure: (10). The antibacterial effect of green nanoparticles with four different concentrations on Escherichia Coli and Staphylococcus aureus

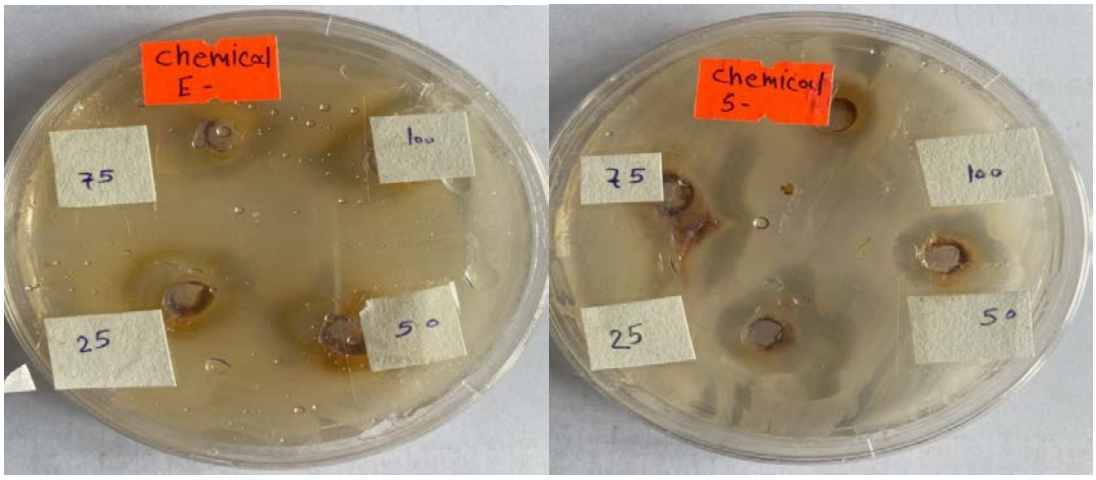

Figure: (11). The antibacterial effect of chemical nanoparticles with four different concentrations on Escherichia Coli and Staphylococcus aureus

CONCLUSION

In this study, Agno3 NPs synthesized by green and chemical synthesis methods were characterized by different techniques to calculate crystallite size, particle size, morphology, spectrophotometry, and antibacterial activity. Different concentrations of silver nanoparticles were studied to inhibit the bacterial activity of two types of bacteria. It was found that green silver nanoparticles were inhibitory to bacterial growth. The average size of the green silver nanoparticles was 19.5 nm, smaller than the chemical silver nanoparticles (30.38 nm), and their optical band gaps were identical. Approximately, spectrophotometry of green silver nanoparticles and chemically synthesized silver nanoparticles shows through spectroscopic data that they stabilize and synthesize silver nanoparticles. Accordingly, green synthesis is more successful, safer and less expensive than chemical synthesis.

ACKNOWLEDGEMENT

The authors thank the University of Omar Al-Mukhtar and Libyan Academy, Al-Jabal Al-Akhdar Branch.

Duality of interest: The authors declare that they have no duality of interest associated with this

manuscript.

Author contributions: Dalal M Ibrahim and Hamad M Idris designed and arranged the structure of the article; Dalal M Ibrahim and Hind M Mohammed performed the experiments; Dalal M Ibrahim, Hamad M Idris, and Hind M Mohammed analyzed the previous work in this field; and Dalal M Ibrahim and Hind M Mohammed wrote the paper. All authors have read and agreed to the published version of the manuscript.

Funding: This research received no external funding.

REFERENCES

Fayaz, A. M., Balaji, K., Girilal, M., Yadav, R., Kalaichelvan, P. T., & Venketesan, R. (2010). Biogenic synthesis of silver nanoparticles and their synergistic effect with antibiotics: a study against gram-positive and gram-negative bacteria. *Nanomedicine: Nanotechnology, Biology and Medicine*, 6(1), 103-109.

Gupta, A., & Silver, S. (1998). Molecular genetics: silver as a biocide: will resistance become a problem? *Nature biotechnology*, 16(10), 888-888.

Huang, J., Liu, J., & Wang, J. (2020). Optical properties of biomass-derived nanomaterials for sensing, catalytic, biomedical and environmental applications. *TrAC Trends in Analytical Chemistry*, 124, 115800.

Ibrahim, D., Abdelghani, K., Anwagy, S., & Rizkallah, R. (2024). Synthesize Iron Oxide and Zinc Oxide Nanoparticles Using Plant Extracts. *AlQalam Journal of Medical and Applied Sciences*, 11-14.

Jadoun, S., Verma, A., & Arif, R. (2020). Modification of textiles via nanomaterials and their applications. Frontiers of textile materials: polymers, nanomaterials, enzymes, and advanced modification techniques, 135-152.

Kalishwaralal, K., Deepak, V., Ramkumarpandian, S., Nellaiah, H., & Sangiliyandi, G. (2008). Extracellular biosynthesis of silver nanoparticles by the culture supernatant of Bacillus licheniformis. *Materials letters*, 62(29), 4411-4413.

Küünal, S., Kutti, S., Rauwel, P., Guha, M., Wragg, D., & Rauwel, E. (2016). Biocidal properties study of silver nanoparticles used for application in green housing. *International Nano Letters*, 6, 191-197.

Küünal, S., Kutti, S., Rauwel, P., Wragg, D., Hussainova, I., & Rauwel, E. (2016). New methodology for the antifungal testing of surfactant-free silver metal nanoparticles for applications in green housing. *Key Engineering Materials*, 674, 133-138.

Küünal, S., Rauwel, P., & Rauwel, E. (2018). Plant extract mediated synthesis of nanoparticles Emerging applications of nanoparticles and architecture nanostructures (pp. 411-446): Elsevier.

Liau, S., Read, D., Pugh, W., Furr, J., & Russell, A. (1997). Interaction of silver nitrate with readily identifiable groups: relationship to the antibacterialaction of silver ions. *Letters in applied microbiology*, 25(4), 279-283.

Nomiya, K., Yoshizawa, A., Tsukagoshi, K., Kasuga, N. C., Hirakawa, S., & Watanabe, J. (2004). Synthesis and structural characterization of silver (I), aluminium (III) and cobalt (II) complexes with 4-isopropyltropolone (hinokitiol) showing noteworthy biological activities. Action of silver (I)-oxygen bonding complexes on the antimicrobial activities. *Journal of inorganic biochemistry*, 98(1), 46-60.

Rai, M., Ingle, A. P., Birla, S., Yadav, A., & Santos, C. A. D. (2016). Strategic role of selected noble metal nanoparticles in medicine. *Critical reviews in microbiology*, 42(5), 696-719.

Rauwel, P., Küünal, S., Ferdov, S., & Rauwel, E. (2015). A review on the green synthesis of silver nanoparticles and their morphologies studied via TEM. *Advances in Materials Science and Engineering*, 2015.

Singh, M., Singh, S., Prasad, S., & Gambhir, I. (2008). Nanotechnology in medicine and antibacterial effect of silver nanoparticles. *Digest Journal of Nanomaterials and Biostructures*, 3(3), 115-122.

Venhoeven, L. A., Bolderdijk, J. W., & Steg, L. (2016). Why acting environmentally-friendly feels good: Exploring the role of self-image. *Frontiers in Psychology*, 7, 207070.

Al-Mukhtar Journal of Basic Sciences 22 (2): 114-122, 2024
Doi: https://doi.org/10.54172/mc14jz12

Research Article **Open Access**

Evaluation of Empty Fava Beans Pods as Bioadsorbent for the Removal of Pb^{2+} from Aqueous Solutions Using Phytoadsorption Technique

Salaheddin A. Sharif[1,*], Widad S. El-Mugrbi[2], Hameda A. M. N. El-Moghrabi[3], Mohamed A. B. Mostafa[4], Adel Alsharkasi[5], Reham B. A.-H. Al Hussein[6], and Khadija A. Abubakr[7]

***Corresponding author:** s.sharif@uob.edu.ly Mercury Research Group, Department of Chemistry, Faculty of Arts and Science, University of Benghazi, Ghemines, Libya.

[2] Department of Botany, Faculty of Arts and Science, University of Benghazi, Ghemines, Libya.

[3] Department of Botany, Faculty of Arts and Science, University of Benghazi, Ghemines, Libya.

[4] Department of Chemistry, Faculty of Science, Tobruk University, Tobruk, Libya.

[5] Department of Statistics, Faculty of Science, University of Benghazi, Benghazi, Libya.

[6] Department of Biology, Faculty of Education, University of Benghazi, Ghemines, Libya.

[7] Department of Biology, Faculty of Education, University of Benghazi, Ghemines, Libya.

Received:
21 April 2024

Accepted:
30 August 2024

Publish online:
31 August 2024

Abstract

Environmental contamination with toxic heavy metals is a global concerne. Cleaning up heavy metals from contaminated aquatic systems forces a lot of challenges. Phytoremediation processes are the interesting safe techniques that were focused by scientists and governments during the last decades for the up-taking of toxic heavy metals from ecosystems. Consequently, phytoadsorption approach was applied in this research using dry empty pods of fava beans (*Vicia faba* L.) to evaluate their potential for the removal of toxic lead heavy metal from its aqueous solutions. We have developed a green and simple method to remove lead ions (Pb^{2+}) from their aquatic system. The obtained results have showed that the 350–1000-µm biomass particles of fava beans pods were able to take up lead ions at highly rated removal percentages and high adsorption capacity using 100-ml, 100-ppm solutions at room temperature and neutral *p*H. For example, the highest removal percentage of lead ions was 66.8% with an absorption capacity of 3.34 mg/g using 2.0 g at a shaking rate of 200 OSC/min after 30 min. On the other hand, the removal percentage of lead ions using 0.1 g of fava beans pods biomass was 36.8 % with the highest absorption capacity of 36.8 mg/g at a shaking rate of 800 OSC/min at the same period of time. Therefore, the empty fava beans (*Vicia faba* L.) pods can be used as potential phytoadsorbents for the removal of lead and other heavy metals from the contaminated aquatic ecosystems.

Keywords: Phytosorption; Dry Empty Fava Beans Pods; Lead Heavy Metal; Aqueous Solutions.

INTRODUCTION

Environmental pollution refers to any negative changes in the ecological balance of the earth's components; land, water and air. These changes can lead to serious phenomena such as climate change which causes major difficulties to the life of all creatures. For example, it can end up with

health risks to humans, animals, and plants. The anthropogenic activities and natural sources are among the main reasons for this contamination. Chemicals, in particular toxic heavy metals, are the most dangerous contaminants to ecosystems, living organisms and therefore to humans (Prasad & Freitas, 2000; Briggs, 2003; Rajakaruna et al., 2006; Zaynab et al., 2022). Heavy metals are elements that have high atomic weights with densities greater than 5 g/cm^3. They are non-biodegradable materials in the environment. Generally, they are found in two groups; essential metals, which have important roles for the biological systems, such as iron (Fe), zinc (Zn), manganese (Mn), cobalt (Co), and copper (Cu). The second type is non-essential metals; which do not have any biological roles but also have toxic effects even at low concentrations, such as arsenic (As), lead (Pb), cadmium (Cd), mercury (Hg) (Chen, 2012; Appenroth, 2010). Volcanic eruptions, forest fires, rock weathering, wind-borne soil particles, and sea-salt sprays represent the natural sources of heavy metals that can be released into the ecosystems. On the other hand, human activities such as domestic wastewater, industrial processes, paints, batteries and textile industry, industrial discharges, agricultural processes, pesticides, fertilizing, mining, and vehicle emissions are the second source of heavy metals (Briggs, 2003; Xiong et al., 2016). The release of heavy metals into the lands and water is a serious threat to agricultural processes and pure groundwater. Exposure to toxic metals can cause a wide variety of diseases and disorders in human, animals and plants. Soft tissues, the brain and nervous system, liver, kidney, and lungs are the most affected organs that can be damaged by exposure to toxic heavy metals, chronically and acutely. Additionally, Alzheimer's disease (AD), Parkinson's disease (PD), Huntington's disease (HD), amyotrophic lateral sclerosis (ALS), Minamata disease, and ataxias are the most well-known neurodegenerative diseases and disorders related to toxic heavy metals (Jaishankar et al., 2014; Breydo & Uversky, 2011).

Generally, the type of heavy metal, its chemical form, dosage, duration and mean of metal exposure, and its solubility in water are the main reasons for heavy metal toxicity. Moreover, accumulation, biomagnification, and resistance to degradation or elimination in live systems are significant factors that lead to an increase the metal toxicity (Aebeed et al., 2022; Ibrahim et al., 2021). Due to the toxic effect of heavy metals in all ecosystems, humans, animals and plants, a lot of efforts to diminish the contamination by heavy metals particularly in the aquatic areas have been afforded. Looking for green solutions such as decontamination or remediation processes for the treatment of water has become a challenge (Ibrahim et al., 2021; Sekhar et al., 2003). The removal of toxic heavy metals from aquatic systems can be achieved using traditional methods such as mechanical, physical or chemical processes. The traditional methods that can be used for removing heavy metals from water are precipitation, ion exchange, membrane processes, evaporation, chemical oxidation or reduction, solvent extraction, chemical fixation, chemical alteration/complexation, capping, membrane filtration, electrochemical treatment technologies, floatation, coagulation, and flocculation (Sekhar et al., 2003; Abdel-Halim et al., 2003; Qadeer & Akhtar, 2005). On the other hand, there are modern methods that have received a lot of attention from governments and international organizations. These methods are based on the functionalization of the biological material and biotechnology. The most interesting approaches are called bioremediation processes (Prasad & Freitas, 2000; Sekhar et al., 2003; Mueller et al., 2009).

The bioremediation process is defined as a simple, innovative, effective, and potentially green technique that utilizes plants, animals or microorganisms to clean up all types of contaminated ecosystems. It is well-known as phytoremediation in the case of using plants as a cleaner (plant-based environmental remediation), or zooremediation for the use of animals. If microorganisms were used in the bioremediation process, then it is known as a microbial remediation (Mueller et al., 2009; Sharif et al., 2023; Sharif et al., 2023). phytoremediation is a cost-effective, efficient, sustainable and green technology that uses plant species to clean up contaminated ecosystems from pollutants to

improve the environment and make it more sustainable (Sharif et al., 2023; Sharif et al., 2023; Ibeanusi et al., 2009; Erdei et al., 2005). Removal of heavy metals from ecosystems (soil or water) by plants using the phytoremediation technology was divided into seven mechanisms depending on the state of the plant. If the plant was alive, there are six mechanisms which are phytoextraction, phytostabilization, phytodegradation, phytovolatilization, phytostimulation (rhizodegradation), and phytofiltration (rhizofiltration). Whereas, it is named as a phytosorption mechanism if the plant is dead. This technique can be further classified into two types; phytoabsorption and phytoadsorption (Sharif et al., 2023; Waoo et al., 2014; Karman et al., 2015).

Phytoadsorption technology is a relatively new, green, simple, and efficient approach that uses the dead cell biomass of plants for the removal of pollutants, in particular toxic heavy metals, from aqueous solutions or industrial wastewaters. Furthermore, it is an inexpensive, sustainable, potential, and profitable process. There is a wide variety of available natural materials such as agri-food wastes (AFW) that were used as adsorbents in the adsorption process (Redha, 2020; Amuda et al., 2007; Hashem., 2007; Shin & Rowell, 2005). The phytoadsorption process was defined as a biological physicochemical interaction between the biomass of plants and the pollutants to remove them from their medium by either physical or chemical adsorption. While the plant biomass, in the physical adsorption mechanism, uses the physical attractions (hydrogen bonding or Van der Waals attractions), it uses the chemical bonding (ionic bonds, and covalent bonds) in the chemical adsorption process on the surface of natural material. There are many factors that play significant roles in the phytoadsorption efficiency. These factors are *p*H, temperature, contact time, biomass dosage, initial metal concentration, presence of another cation, and chemical modifications of biosorbents. This technique was widely used for removing heavy metals from their aquatic systems onto the surface of dead plant particles (Redha, 2020; Rahman & Sathasivam, 2015; Salim et al., 2021; Dubey et al., 2014; Etorki et al., 2014).

In this study, we aimed to assess the potential of dry empty fava bean pods as phytoadsorbent for the removal of lead heavy metal ions from their aqueous solutions using the phytoadsorption technique.

MATERIALS AND METHODS

Sample Preparation

Lead Metal (Pb^{2+})

A 100-ppm lead metal ions solution was prepared by dissolving lead nitrate, $Pb(NO_3)_2$, in distilled water. This concentration was used in all experiments thereafter.

Biomass of Empty Fava Beans Pods

Fresh fava beans were collected from the local market, in Benghazi city, Libya. The fava bean pods were emptied from seeds, washed with water, and dried in a dark place for 2 months. Next, they were ground and an amount of 350−1000-μm particles were sieved with two sieves. The dry particles were then stored in a dark and dry place for the next steps.

Phytoadsorption Experiments and Analysis of Samples

All experiment procedures and samples analyses were carried out according to standard methods (Sharif et al., 2023; Sharif et al., 2023). Different amounts of empty fava beanspod particles, 2.0, 1.0, 0.50, or 0.10 g, were separately added to 100 mL of the 100-ppm lead nitrate solution of each sample in a 500-mL container (polyethylene bottle). Then, they were shaken well using an instrumental shaker (Flask Shaker SF1) at various shaking rates of 200, 400, 600, and 800 OSC/min for

30 minutes. All experiments were conducted at room temperature and a neutral *p*H. All bottles of the lead-fava beans powder mixtures were left for 24 hours to allow the solid matter to precipitate. Next, the precipitated mixtures were filtered using the Whatman filter papers No 1. The filtrates were then diluted to 1 ppm and acidified with nitric acid (0.5 mL of 60% HNO_3) at a rough *p*H of 3, and stored in the refrigerator for the next steps. Concentrations of the remained lead metal ions in all filtrates were detected using the flame atomic absorption spectroscopic (FAAS) instrument (Model: Perkin Elemer 500) at a room temperature of 24 °C and a *p*H of solutions at 2.5–3.6. Eventually, the removal percentage (%) of lead ions and the adsorption capacity q_e (mg/g) were calculated. The adsorption capacity of each sample after equilibrium was calculated by the mass balance relationship equation as follows

$$q_e = (C_i - C_d)\, V/W$$

where C_i is the initial concentration of lead ion solution (mg/L), C_d is the detected concentration of filtrate solutions (mg/L), V is the volume of the solution (L) and W is the mass of adsorbate (g).

RESULTS AND DISCUSSION

All investigated samples showed that the empty fava bean pods, which are used as bioadsorbent, with a size of 350−1000 μm were efficiently able to remove significant amounts of lead ions from their aqueous solutions. This depends on many studied factors such as loaded biomass, and shaking rate at a contact time of 30 minutes. These observations were due to the high affinity of biomass surface to adsorb the lead ions.

Shaking Rate: 200 OSC/min

Various amounts of biomass loading (2.0, 1.0, 0.5, and 0.1 g) were investigated during 30 minutes of shaking. Generally, there was a fluctuation in the observed removal percentages of lead ions (Table 1, Figure 1). For example, the removal percentage of lead ions using 2.0 g of fava bean pods was 66.8% after 30 minutes of shaking (entry 1). This result represents the highest removal percentage within all samples. The adsorption capacity of this experiment was 3.34 mg/g. Next, the removal percentage decreased to 21.4% with an adsorption capacity of 2.14 mg/g due to the use of 1.0 g of biomass at the same period of time (entry 2). This represents the least adsorption capacity of all conducted samples. Unexpectedly, although the loading of the dry fava beans pods was decreased to 0.5 g the removal percentage of lead ions was raised to 44.9% with a significant increase in the adsorption capacity with 9.98 mg/g (entry 3). Eventually, by decreasing the biomass loading to 0.1 g, the removal percentage of lead ions decreased to 18.8% with a remarkable increase in the adsorption capacity of dry fava bean particles to 18.8 mg/g (entry 4).

Shaking Rate: 400 OSC/min

Similarly, different amounts of biomass (2.0, 1.0, 0.5, and 0.1 g) were investigated during the same interval time of shaking (30 minutes). The observed results of these experiments showed the same pattern of the removal percentages (Table 1, Figure 1). For instance, the removal percentage of lead ions by using 2.0 g of the dry fava beans pods was 56.6% after 30 minutes of shaking (entry 5). This result represents the highest removal percentage within this group. The adsorption capacity of this experiment was 2.83 mg/g. Next, the removal percentage decreased to 38.6% with an adsorption capacity of 3.86 mg/g due to the use of 1.0 g of biomass at the same period of time (entry 6). Afterward, when the loading of the dry fava beans pods was decreased to 0.5 g, the removal percentage of lead ions was raised to 47.1% with a significant increase in the adsorption capacity to 9.42 mg/g (entry 7). At the lowest amount of biomass loading with 0.1 g, the removal percentage of lead ions decreased to 26.3% with a remarkable increase in the adsorption capacity of dry fava

beans particles into 26.3 mg/g (entry 8). These results were consistence with the previous observations of the 200 OSC/min shaking-experiments.

Shaking Rate: 600 OSC/min

Using the same amounts of dry fava bean particles (2.0, 1.0, 0.5, and 0.1 g), four experiments were conducted at the same period of time (30 minutes). The observed results in these experiments showed a gradual decrease in the removal percentages of lead ions with the decreased load of dead biomass (Table 1, Figure 1). For example, the Pb-removal percentage using 2.0 g of the dry fava beans pods was 54.9% after 30 minutes of shaking (entry 9). This result represents the highest removal percentage within this group as expected. The adsorption capacity of this experiment was 2.75 mg/g. Next, the removal percentage decreased to 37.6% with an adsorption capacity of 3.76 mg/g due to the use of 1.0 g of biomass at the same period of time (entry 10). Interestingly, when the loading of the dry fava beans pods was decreased to 0.5g the removal percentage of lead ions was decreased to 29.6% with a significant increase in the adsorption capacity of 5.92 mg/g (entry 11). Consistently, at the lowest loading of biomass (0.1 g), the removal percentage of lead ions decreased to 28.7% with a remarkable increase in the adsorption capacity of dry fava bean particles into 28.7 mg/g (entry 12).

Shaking Rate: 800 OSC/min

Similarly, the same amounts of biomass (2.0, 1.0, 0.5, and 0.1 g) were also investigated for the highest shaking rate during the same contact time (30 minutes). The observed results of these samples showed the same pattern of the removal percentages of all the previous experiments (Table 1, Figure 1). For example, the removal percentage of lead ions using 2.0 g of the dry fava beans pods was 53.1% after 30 minutes of shaking (entry 13). The adsorption capacity of this experiment was 2.66 mg/g. Next, the removal percentage decreased to 40.8% with an adsorption capacity of 4.08 mg/g due to the use of 1.0 g of the biomass at the same period of time (entry 14). Next, with 0.5 g loading of the dry fava beans pods the removal percentage of lead ions increased to 48.6% with an increase in the adsorption capacity of 9.72 mg/g (entry 15). Finally, at the lowest loading of fava beans biomass, 0.1 g, the Pb-removal percentage decreased to 36.8% (entry 16). The calculated adsorption capacity of dry fava bean particles using this amount of material was 36.8 mg/g. This result represents the highest adsorption capacity within all conducted experiments.

Table: (1). The removal percentage of Pb^{2+} (%) and adsorption capacity, q_e, (mg/g) after shaking using dry empty fava beans pods.

Entry	Biomass (g)	Shaking Rate(OSC/min)	Pb Detected (ppm)	Pb Detected(%)	Pb Removal (%)	Adsorption Capacity (mg/g)
1	2.0	200	33.2	33.2	66.8	3.34
2	1.0	200	78.6	78.6	21.4	2.14
3	0.5	200	55.1	55.1	44.9	8.98
4	0.1	200	81.2	81.2	18.8	18.8
5	2.0	400	43.4	43.4	56.6	2.83
6	1.0	400	61.4	61.4	38.6	3.86
7	0.5	400	52.9	52.9	47.1	9.42
8	0.1	400	73.7	73.7	26.3	26.3
9	2.0	600	45.1	45.1	54.9	2.75
10	1.0	600	62.4	62.4	37.6	3.76
11	0.5	600	70.4	70.4	29.6	5.92
12	0.1	600	71.3	71.3	28.7	28.7
13	2.0	800	46.9	46.9	53.1	2.66
14	1.0	800	59.2	59.2	40.8	4.08
15	0.5	800	51.4	51.4	48.6	9.72
16	0.1	800	63.2	63.2	36.8	36.8

Conditions: Pb^{2+} concentration = 100 ppm. Particle size of dry empty fava beans pods: 350–1000 μm. Contact time: 30 min. Bottle volume: 500 mL. Sample volume: 100 mL.

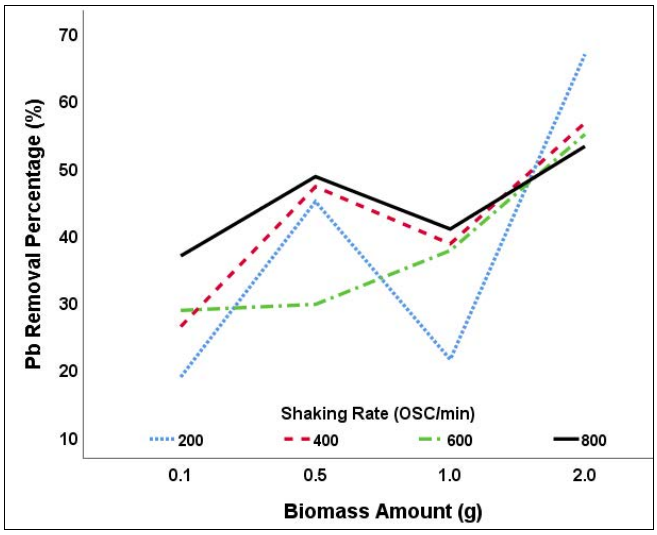

Figure: (1). The removal percentage of Pb^{2+} (%) after shaking using dry empty fava beans pods.

Adsorption Capacity of Fava Beans Pods

The adsorption capacity, q_e, of dry fava bean pods for the removal of lead ions from their aqueous solutions was gradually decreased from using 0.1 to 2.0 g of the biomass (Figure 2). It was observed that the shaking rate of 800 OSC/min afforded the highest adsorption capacity of the 0.1 g ground fava bean pods. Then the adsorption was sharply decreased due to using 0.5 g of the dry biomass, followed by a gradual decrease in the capacity with increasing the amount of bioadsorbent that was used. Similarly, the applied shaking rates have shown that the pattern of adsorption capacity of the dry particles of fava bean pods was in inverse proportion with the biomass loading.

To our knowledge, this work is the third attempted report for the investigation of the dry empty fava beans pods as bioadsorbent for the removal of lead ions from aqueous solution (Naji et al., 2019; Sánchez-Ponce et al., 2022). According to Naji, the removal percentage of lead ions from their 100 mL synthetic wastewater solution using 1 g of the dry fava bean pods (<1000 μm) was around 68, 70, and 80% after 1, 2, and 4 hours of shaking (125 OSC/min), respectively, at *p*H 5. [30] Recently, it was reported that the removal percentage of Pb^{2+} using 0.5 g of empty broad beans pods (<125 μm) was 91.5% with an adsorption capacity of 15.62 mg/g from50 mL, 1 ppm of lead ions solution after 24 hours of shaking using an orbital laboratory shaker (200 rpm). However, these observations were not optimized during that study (Sánchez-Ponce et al., 2022).

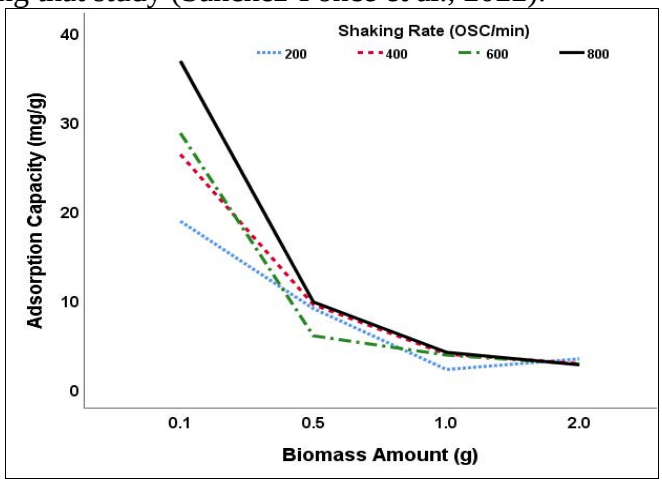

Figure: (2). The adsorption capacity, q_e, (mg/g) of dry empty fava beans pods for the removal of Pb^{2+}.

CONCLUSION

Contamination of aquatic systems with heavy metals has become a dangerous threat to humans, animals and plants. Removal of these pollutants required continuous developments of green technologies. Recently, the phytoadsorption process has been proved as a well-known, green, potential and sustainable approach for the removal of heavy metals using a wide variety of natural materials plants. The obtained data from the designed experiments have shown that the dead biomass of empty fava bean pods can be used as efficient phytoadsorbents for the removal of lead heavy metal ions from their aqueous solutions at low concentrations.

ACKNOWLEDGEMENT

The authors would like to thank Dr Najwa H. Ansir, and Rehab N. Daggari (MSc), Department of Chemistry, Faculty of Science, for providing the Instrumental Shaker (Flask Shaker SF1). The authors would like also to thank Dr Hussein B. Jenjan, Department of Zoology, Abdusslam Elmogasapi, Department of Botany, Salh Ahmed Alsunousi, Department of Chemistry, Faculty of Science, and Khaled Ali Jhawi, Faculty of Arts and Science - Ghemines for their help and providing all necessary facilities. The authors are also thankful to Farag M. Ali, Quality Control Specialist, Water Quality Control Department, Man-Made River Project, Benghazi–Libya, for conducting the atomic absorption analysis.

Duality of interest: No potential conflict of interest was reported by the authors.

Authors' Contributions: All authors contributed to data analysis, drafting, and revising of the paper and agreed to be responsible for all aspects of this work.

Funding: Authors have not received any type of funding for the work reported in this manuscript.

REFERENCES

Abdel-Halim, S.H., Shehata, A.M.A. and El-Shahat, M.F. (2003). Removal of Lead Ion from Industrial Wastewater by Different Types of Natural Materials. *Water Research, 37*,1678–1683.

Aebeed, A.S., Sharif, S.A., Amer, A.H., Jibreel, A.M., Alsoaiti, S.F. (2022). Growth and Reproduction of the Earthworm After Exposure to Eisenia fetida Sub Lethal Concentration from Remilitine and Lead Mixture. *SJUOB, 35*,199–203.

Amuda, O.S., Giwa, A.A., Bello, I.A. (2007). Removal of Heavy Metal from Industrial Wastewater Using Modified Activated Coconut Shell Carbon. *Biochemical Engineering Journal, 36*, 174–181.

Appenroth, K.J. (2010). Definition of “heavy metals” and their role in biological systems, Soil heavy metals. *Springer*, 19–29.

Breydo, L., Uversky, V.N. (2011). Role of metal ions in aggregation of intrinsically disordered proteins in neurodegenerative diseases. *Metallomics*, 2011, *3*,1163–1180.

Briggs, D. (2003). Environmental pollution and the global burden disease. *British Medical Bulletin, 68*, 1–24.

Chen., J.P. (2012). Decontamination of heavy metals: processes, mechanisms, and applications, 1st Ed., CRC Press, New York.

Dubey, A.M.S.S.A., Mishra, A., Singhal, S. (2014). Application of dried plant biomass as novel low-cost adsorbent for removal of cadmium from aqueous solution. *International Journal of Environmental Science and Technology, 11*, 1043–1050.

Erdei, L., Mezôsi, G., Mécs, I., Vass, I., Fôglein, F., Bulik, L. (2005). "Phytoremediation as a program for decontamination of heavy-metal polluted environment," in Proceedings of the 8th Hungarian Congress on Plant Physiology and the 6th Hungarian Conference on Photosynthesis, *49*, 75–76.

Etorki, A.M., El-Rais, M., Mahabbis, M.T., and Moussa, N.M. (2014). Removal of some heavy metals from wastewater by using of fava beans. *Am. J. Anal. Chem., 5*, 225–234.

Hashem, M.A. (2007). Adsorption of Lead Ion from Aqueous Solution by Okra Wastes. *International Journal of Physical Science*, *2*, 178–184.

Ibeanusi, V.M., Grab, D. A., In collaboration with Jensen, L., Stephen Ostrodka, S. (2004) Environmental Protection Agency. Radionuclide Biological Remediation Resource Guide, U. S. Environmental Protection Agency.

Ibrahim, M.A., Sabti, M.Z., Mousa, S.H. (2021). In vitro accumulation potentials of heavy metals in big-sage (Lantana camara L.) plant. *DYSONA – Life Science*, *2*(2), 12–17.

Jaishankar, M., Tseten, T., Anbalagan, N., Mathew, B.B., Beeregowda K.N. (2014). Toxicity, mechanism and health effects of some heavy metals. *Interdisciplinary Toxicology*, *7*, 60–72.

Karman, S.B., Diah, S.Z.M., Gebeshuber, I.C. (2015). Raw Materials Synthesis from Heavy Metal Industry Effluents with Bioremediation and Phytomining: A Biomimetic Resource Management Approach. *Advances in Materials Science and Engineering*, Volume 2015, Article ID 185071, 21 pages.

Mueller, J.G., Cerniglia, C.E., Pritchard, P.H. (2009). Bioremediation of Environments Contaminated by Polycyclic Aromatic Hydrocarbons. In Bioremediation: Principles and Applications, Cambridge University Press, Cambridge.

Naji, A.M., Kareem, S.H., Nief, O.A., Flaeeh, H.C. (2019). Fruit and Agricultural Waste Cortex as Natural Resins Adsorbents for Removal of Heavy Metal Ions from Waste Water. *Plant Archives*, 19, *2*, 966–971.

Prasad, M.N.V., Freitas, H. (2000). Removal of toxic metals from solution by leaf, stem and root phytomass of *Quercus ilex* L. (holly oak). *Environ. Pollution*, *110*, 277–283.

Qadeer, R., Akhtar, S. (2005). Study of Lead Ion Adsorption of Active Carbon. *Turk. J. Chem., 29*, 95–99.

Rahman, M., Sathasivam, K.V. (2015). Heavy metal adsorption onto Kappaphycus sp. from aqueous solutions: the use of error functions for validation of isotherm and kinetics models. *BioMed research international*, Volume 2015, Article ID 126298.

Rajakaruna, N. Tompkins, K.M., Pavicevic, P.G. (2006). Phytoremediation: An Affordable Green Technology for the Clean-up of Metal-Contaminated Sites in Sri Lanka. *Cey. J. Sci. (Bio. Sci.)*, *35*, 25–39.

Redha, A.A. (2020). Removal of heavy metals from aqueous media by biosorption. *Arab Journal of basic and applied sciences*, *27*, 183–193.

Salim, R.M.D., Asik, J., Sarjadi, M.S. (2021). Chemical functional groups of extractives, cellulose and lignin extracted from native Leucaena leucocephala bark. *Wood Sci. Technol.*, *55*, 295–313.

Sánchez-Ponce, L., Díaz-de-Alba, M., Casanueva-Marenco, M.J., Gestoso-Rojas, J., Ortega-Iguña, M., Galindo-Riaño, M.D., Granado-Castro, M.D. (2022). Potential Use of Low-Cost Agri-Food Waste as Biosorbents for the Removal of Cd(II), Co(II), Ni(II) and Pb(II) from Aqueous Solutions. *Separations*, *9*(10), 309–.

Sekhar, K.C., Kamala, C.T., Chary, N.S., Anjaneyulu, Y. (2003). Removal of heavy metals using a plant biomass with reference to environmental control. *Int. J. Miner. Process*, *68*, 37–45.

Sharif, S.A., El-Moghrabi, H.A.M.N., El-Mugrbi, W.S., Alhddad, A.I. (2023). Fava Beans (Vicia faba L.) Phytosorption of Pb^{2+} Ions from its Aqueous Solutions. *Asian J. Green Chem.*, *7*, 85–90.

Sharif, S.A., El-Mugrbi, W.S., Alhddad, A.I., El-Moghrabi, H.A.M.N., Elarfy A.R., Alshahopy, N.A. (2023). Removal of Toxic Lead Ions from their Aqueous Solutions Using Fava Beans Phytoadsorption Technique. *AlQalam Journal of Medical and Applied Sciences*, Special Issue for 6th International Conference in Basic Sciences and Their Applications (6th ICBSTA, 2023), P: 71–86, 2/12/2023

Shin, E.W., Rowell, R.M. (2005). Cadmium Ion Sorption onto Lignocellulosic Biosorbent Modified by Sulfonation: The Origin of Sorption Capacity Improvement. *Chemosphere*, *60*, 1054–1061.

Waoo, A., Khare A.S., Ganguli, S. (2014). Comparative Tissue Culture Studies on Lantana Camara and Datura Inoxia at Heavy Metal Contaminated Site and Phytoremediation Approach at Industrially Contaminated Sites. *International Journal of Advances in Biology*, *1*, 55–62.

Xiong, T., Dumat, C., Pierart, A., Shahid, M., Kang, Y., Li, N., Bertoni, G., Laplanche, C. (2016). Measurement of metal bioaccessibility in vegetables to improve human exposure assessments: field study of soil–plant–atmosphere transfers in urban areas, South China. *Environ. Geochem. Health*, *38*, 1283–1301.

Zaynab, M., Al-Yahyai, R., Ameen, A., Sharif, Y., Ali, L., Fatima, M., Khan, K.A., Li, S. (2022). Health and environmental effects of heavy metals. *J. King Saud Univ. Sci.*, *34*, 101653.

Al-Mukhtar Journal of Basic Sciences 22 (2): 123-133, 2024
Doi: https://doi.org/10.54172/cqtrdm38

Research Article **Open Access**

Evaluation of Stability constant of Binary complex of Tannic Acid with Fe(II) in Aqueous Solution: Potentiometric Study

Nouria A. Shnin[1], Aziza K. Haiwdi[2], Mohamed Zidan[3] and Aisha A. AL-Abbasi [*]

***Corresponding author:** ais.alabbasi@sebhau.edu.ly, Department of Chemistry, Faculty of Science, University of Sebha, Libya.

[1, 2, 3] Department of Chemistry, Faculty of Science, University of Sebha, Libya.

Received:
14 May 2024

Accepted:
25 August 2024

Publish online:
31 August 2024

Abstract
Tannic acid as a polyphenol has biological and pharmacological activities, as well as its ability to bond to a wave of transition metals. In this study, the protonation equilibria of the tannic acid were determined and used for determining the stability constants of the binary complexes formed with iron (II) ions in the aqueous medium under the experimental conditions by the potentiometric method using Irving and Rossotti equation, where Stability constant was 3.205 for Fe(II)–tannic acid complex. In contrast, Fe(II) formed complexes with tannic acid of various stoichiometries, which in the 1:1 molar ratio at pH = 11.24. Furthermore, the ionic strength and the influence of temperature on the stability of the complexes are investigated, where stability constant in the presence of 0.1 M NaCl (ionic strength) of binary iron-Tan complex equal 3.254, and at different temperatures were log K1= 3.156 at 298.15 K, log K1 = 3.205 at 310.15 K, and log K1= 3.256 at 313.15 K.

Keywords: Ferrous ions; Formation constant; Binary complexes; potentiometry; tannic acid

INTRODUCTION

The majority of most living organisms depend on iron as a necessary mineral element since it is considered essential to all life and existence. It can be found in most nutrition bases (Abbaspour et al., 2014). The right amount of gin is produced by the body to minimize iron production; too much or too little causes an imbalance in the body. As the protein that carries oxygen to all of the body's cells and organs, hemoglobin needs iron to function (McGee, 2017). It also functions as a catalyst for many other enzymes, including catalase (Kadiiska et al., 1995). A newborn child's body has 0.5 grams of iron, compared to 4-5 grams for an adult male and roughly 3 grams for a female's body (Moustarah & Daley, 2024). The majority of this amount 65% is found in red blood cells, specifically in hemoglobin. The remaining 25% is found in iron reserves, such as ferritin or hemosiderin, and the other 10% is found in muscles, specifically in myoglobin (McDermid & Lönnerdal, 2012, Kaufman et al., 2024).

Many foods include two different forms of iron: non-heme iron, which is found in grains, vegetables, fortified foods, nutritional supplements, eggs, almonds, and green vegetables, particularly spinach; and heme iron, which is associated with hemoglobin and myoglobin (Hurrell & Egli, 2010). Heme iron is bioavailable (15–35%) and is not significantly affected by dietary variables, but non-heme iron absorption is significantly lower (2–20%) and extensively influenced by other food components (Piskin et al., 2022). However, in most meals, non-heme iron is far more plentiful

in the diet than heme iron. Despite its lower bioavailability, non-heme iron makes a greater contribution to iron nutrition than heme iron. The substances that inhibit iron absorption comprise polyphenols, calcium, and photic acid (Ems & Huecker, 2019).

Many types of plant material include tannin. Galatannin is the chemical component that makes up most natural tannin (Cotoraci et al., 2021). It contains a complicated compound that is fundamentally made up of one glucose molecule bound to up to five digallic acid molecules, as seen in Figure 1 (Fu & Chen, 2019). The tannin molecule hydrolyzes in a water solution to produce glucose and digallic acid. Tannic acid's acidic qualities are derived from the carboxyl hydrogen found inside the digallic acid molecule. One particular kind of tannin, a kind of polyphenol, is tannic acid. The various phenol sets in the molecule are the source of its low acidity (pK_a of about 6). This formula is equivalent to decagalloyl glucose. The above system represents the tannic acid utilized in those tests, which has a molecular weight of 322 (Fu & Chen, 2019). To reduce bleeding, people apply tannic acid to the area where they have been exposed, especially to cold sores and fever blisters, diaper rash and prickly heat, poison ivy, ingrown toenails, sore throat, sore tonsils, spongy or receding gums, and skin rashes.

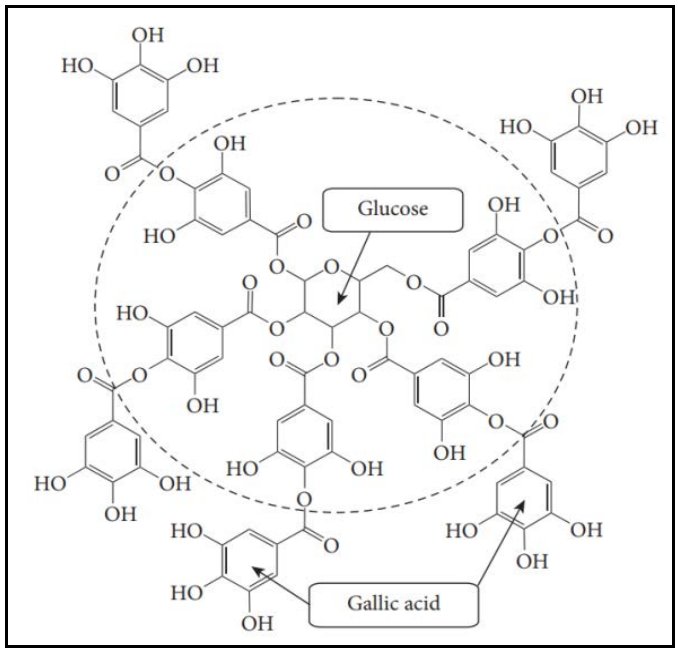

Figure (1). Configuration of tannic acid (Fu & Chen, 2019)

Oral tannic acid treatment is available for bleeding, dysentery, prolonged diarrhea, bloody urine, aching joints, persistent coughing fits, and cancer (Chen et al., 2022). Over the past ten years, there has been a growing usage of tannic acid (Tan), an antioxidant present in plants, in biomedical research.(Maharani et al., 2022). Tannic acid extracted from the galls of oak trees has been used for ages in various important applications (Maharani et al., 2022). Tan's application in Tan is based on its hydrogen bonding properties with proteins and other biomolecules, as well as its abundance of hydroxyl groups, which provide it versatility (Baldwin & Booth, 2022). Huge, subdued-colored molecules that exhibit colloidal behavior can be found in combinations of tannic acid and iron (Ahmad, 2014).

There are some Factors affecting the stability of metal compensation such as solvent, temperature (which has an impact on the values of stability constant) and the nature of ligands. In a prior study,

the potentiometric approach was to estimate the stability constants of binary complexes generated from iron (II) ions with tannic acid as our controversial motive for exploring the behavior of metal ions in aqueous solution (Al-abbasi A., 2023, Al-abbası A., 2023, Belkher, 2019 , Al-abbasi et al., 2022, Suhud et al., 2015, Khalifa, 2018, Dnkm et al., 2024). Additionally, the exploring the effect of temp. and ionic strength of NaCl on the formed complex and calculating thermodynamic parameters.

MATERIALS AND METHODS

Chemicals and Instrumentations

All chemicals and materials were of reagent grade or the highest quality commercially available and were used without further purification: Tannic acid (BDH Chemicals, 99%), ferrous Chloride (Carlo Erba, 99.8 %), Sodium Hydroxide (Shandong China), 98.8%), Sodium Chloride (BDH Chemicals, 99.7%), Hydrochloride (Scharlau chemise, 36%). The devices used are all from well-known companies: Balance (Mettlertoledo/Al204), Thermostat Water Bath (Grant Instrument, England), Conductivity/ pH-meter (Thermo Electron/Orion3 Star (PH Benchtop)/USA).

Preparation of Standard Solutions

Ferrous chloride (0.176 g) was dissolved in a standard beaker (100 mL), and the volume was filled with distilled water (deionized) up to the mark to obtain a concentration of 0.01M. Other concentrations of 0.001 M and 0.005 M were obtained. Tannic acid (0.176 g) was dissolved in a standard flask with a capacity of 100 mL, and the volume was filled with distilled water up to the mark to obtain a concentration of 0.01 M, from which other concentrations (0.005 M) were obtained. 0.001 M. A solution of (0.1 M) sodium hydroxide was prepared by dissolving the requisite quantities (2 g) with distilled deionized water. The solution of sodium hydroxide was standardized by titrating against the standard oxalic acid solution. The solution was used as the titrant for the pH-metric titrations. Sodium chloride solution (0.1 M) was prepared by dissolving 1.461 g of NaCl in a standard 250 mL beaker and filling the volume up to the mark with distilled (deionized) water.

Effect of temperature and ionic strength on the formation of binary complex

The temperature effect on the binary and ternary complexes was studied pH-metrically at temperatures of 293.15 K, 298.15 K, 303.15 K, 310.15 K and 313.15 K and 0.004 M metal ion concentration. The stability constant was determined at each temperature, and its values can be correlated with Δ*G* (free energy), Δ*H* (enthalpy), and Δ*S* (entropy). The potential and conductivity measurements were performed in the presence of a strong electrolyte of NaCl. This study was conducted to determine the effect of adding 0.1 M sodium chloride (NaCl) on the formation of the complexes at a temperature of 313.15 K.

RESULTS

Formation constants of the ligands

Dissociation constants of Ascorbic acid, Glutamine, and Tannic acid were investigated by titration titrations using sodium hydroxide. The following curves were constructed using the titration data:

i. Free Acid (HCl) Curve
ii. the free acid+ Tannic acid (HCl+ Tan) Curve.

$$HL \overset{K_1^H}{\rightleftarrows} H^+ + L^- \quad (1)$$

$$K_1^H = \frac{[H^+][L^-]}{[HL]} \quad (2)$$

Values of n_A (average number of protons attached to each ligand) were determined according to Irving and Rossotti as shown in Eq. 3:

$$\bar{n}_A = Y + \frac{(V' - V'') \times (N - E^o)}{(V^o - V') \times T_L^o} \qquad 3$$

Where: $\bar{n}_A$ is the average number of protons bound per not complex bound ligand molecule, y is the number of the replaceable hydrogen atoms from the ligand, V^O is the initial total volume of solution, V' and V'' are the volume of alkali required to attain the same pH in the acid curve and same pH in the (acid + ligand) curve, respectively, N is the concentration of alkali, E^o and T_L^O are the initial concentration of HCl acid and the total ligand concentration, respectively. The pH value corresponding to n_A= 0.5, 1.5, 2.5, 3.5, and 4.5 is represented by the values of $\log K_1^H$, $\log K_2^H$, $\log K_3^H$, and $\log K_4^H$ (the ligands' proton dissociation constants) as shown in (Table 1).

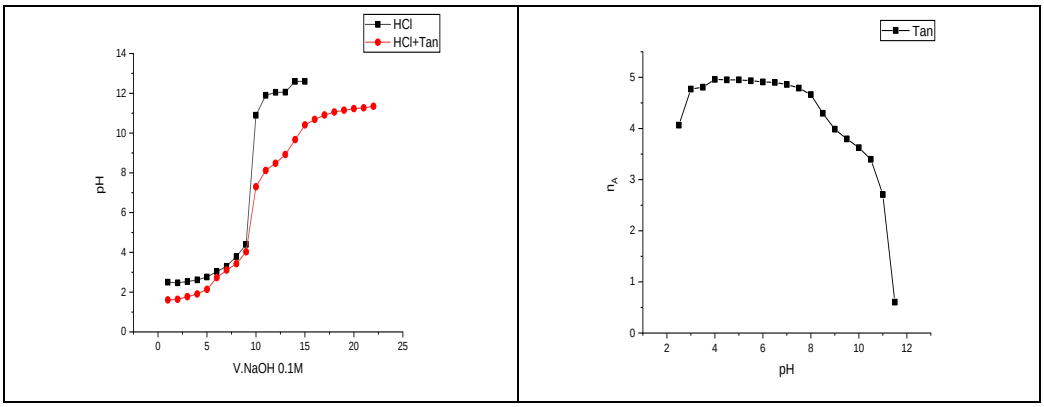

Figure (2). Potentiometric titration curves and Protonation constant curves of 0.01M Tannic Acid at 310.15 K

According to the Irving Rossetti equation, Figure 2 shows how the correlates' dissociation constants can be calculated from the pH value corresponding to their n_A values at (0.5, 1.5, 2.5 values). For Tannic acid, the $\log K_1^H$, $\log K_2^H$, $\log K_3^H$, and $\log K_4^H$ values are given by the pH values corresponding to 1.5, 2.5, 3.5 and 4.5 values. As for Tannic acid, it shows similarity in the recorded values, but a difference appears in the number of protons given, in which the results recorded in this study showed that the Tannic acid gives four protons, while the previous study showed that it gives only two protons (Zheng et al., 2016).

Table (1). Values of dissociation constants of Tan at 310.15K

298.15 K	310.15 K	313.15K
K_{a1}=11.65	K_{a1} =11.51	$K_{a1=}$ 12.5
K_{a2} =11.08	K_{a2} =11.3	K_{a2} = 12. 0
K_{a3} = 10.15	K_{a3} = 11.08	K_{a3}= 11.15
K_{a4} = 8.05	K_{a4} = 10.35	K_{a4} = 9.1
K_{a5} = 6	K_{a5} = 8.2	K_5= 7.0
K_{a6}=/	K_{a6} = 2.4	K_6= 2.3

Binary complex of ferrous Tennate

The stability of complexes of iron (Fe^{+2}) with different bioactive Tannic acids was studied by the potentiometric method. This study was done by forming this complex in an aqueous solution in the presence and absence of ionic strength of sodium chloride at a body temperature of 37 °C under certain conditions of concentration. Formation constants of Iron (Fe^{+2}) binary complex Tannic acid were studied by potentiometric titrations using sodium hydroxide. The following curves were constructed using the titration data:

1) Free acid curve

2) free acid + Tan
3) free acid+ Tan + Fe^{+2}

Following equations were used to compute $\bar{n}$ (average number of ligand molecules attached) and p_L (free ligand exponent) as revealed by Irving and Rossotti (Almbrok, 2023; Irving & Rossotti, 1954; Irving, 1953):

$$n_L = \frac{(V''' - V'''') \times (N - E^\circ)}{(V^\circ - V''') \times T_M^o \times \bar{n}_A} \qquad 4$$

$$pL = \log[\frac{1 + pK_1^H[H^+] + pK_1^H \cdot pK_2^H([H^+])^2}{T_L^\circ - \bar{n}T_M^\circ} \times \frac{V^\circ + V'''}{V^\circ}] \qquad 5$$

Where $\bar{n}_A$ is the average number of protons bound per not complex bound ligand molecule, V^o is the initial total volume of solution, V', V'' and V''' are the volume of alkali required to attain the same pH in the acid curve, same pH in the (acid + Tan) curve and volume of alkali required to attain the same pH in the (acid+ Fe^{+2} + Tan) curve respectively, N is the concentration of alkali, E^o and T_L^o are the initial concentration of HCl acid and the total ligand concentration, respectively, T_M° is total metal ion concentration.

The stability constant of ferrous binary complexes with Tan ligands were investigated potentiometrically. The effect of changing the concentration of ferrous ion on stability constants of binary complexes were investigated by using different concentrations of 0.001 M, 0.005 M and 0.01 M of ferrous ion at 310.15 K. According to Irving and Rossotti calculations; the $\bar{n}$ and p_L values at the ferrous ions concentration of 0.005 M and 0.001 M were all negative. As a result, the formation constants at that concentration could not obtained and the 0.01M was chosen for studying the formation constant of ferrous binary complexes of Asc, Glut and Tan ligands. The stability constants of the ferrous tannate complex at 310.15K were found to be 3.205 at pH 11.14

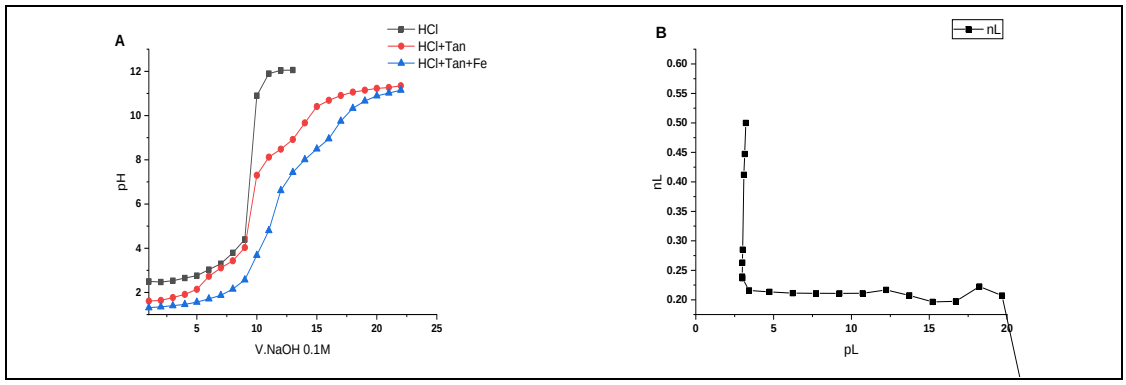

Figure (3). Potentiometric titration (A), and Protonation constant Curves (B) of ferrous- Tan complex at 0.01M

The following general observations can be made: (i) The metal solutions employed in the present investigation are dilute (1×10^{-2} M); (ii) Proton release upon the formation of the metal ion complexes with the ligand was indicated by shifting the metal ion titration curves to the right-hand side of the ligand titration curve along the alkali volume axis (Al-Saidi et al., 2020). The Tannic acid binary complex, only shows one formation constant at pH = 11.24. the other formation constant might be found at pH higher than 13, which is cannot detected in our experiments pH.

Curves (Figure 3) and equations (4 & 5) were utilised to determine the values of nL, pL. The metal ion titration curves were moved to the right-hand side of the ligand titration curve along the alkali volume axis, referring to proton release upon formation of the metal ions complexes with the ligand [15]. The tannic acid binary complex only displays one formation constant at pH = 11.24 and log K = 3.205; the other formation constant may be found at pH higher than 13, which is not detected in

our experiment's. The values of nL, pL obtained for the iron-Tan stoichiometric system indicate the formation of 1:1 complexes, and they were related to the following equilibrium equations 6 & 7:

$$M^{+} + L^{-} \underset{}{\overset{K_1}{\rightleftharpoons}} ML \qquad 6$$

$$K_1 = \frac{[ML]}{[M^{+}][L^{-}]} \qquad 7$$

Protons attaching to Tan's hydroxide group with metal ions to create complexes is related to the log K_1 value.

Ionic strength

To study the effect of ionic strength on the dissociation constant of Tan and the stability constant of its corresponding complex; a fixed concentration of each ligand (0.01 M) was chosen, and the dissociation constants were studied in the presence of a fixed concentration of sodium chloride (0.1 M) by titrations with sodium hydroxide, where the titrations data were used to build the following curves: Free Acid + NaCl, free acid + Tan acid + NaCl, The free acid + Tannic acid + Fe^{+2} + NaCl as shown in Figure 4.

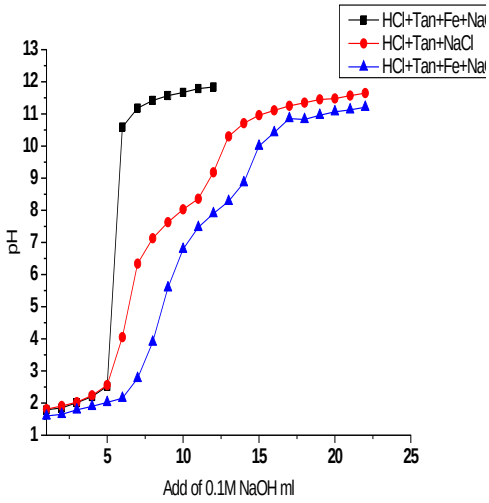

Figure (4). Potentiometric of Tan and its complex in the presence of 0.1M NaCl at 310.15K

Figure 4 shows the potentiometric titration curves in the presence and absence of NaCl by using Irving Rosseti's method. The obtained values of the dissociation constants are presented in Table 2.

Table (2). Dissociation constant and stability constant of Tan and ferrous tannat at 310.15K in the presence and the absence of NaCl

Comp.	Log K_a	Log K_a in 0.1M NaCl
Tan	K_{a1} =11.51 K_{a2} =11.3 K_{a3} = 11.08 K_{a4} = 10.35 K_{a5} = 8.2 K_{a6} = 2.4	K_{a1} =11.45 K_{a1} = 11.08 K_{a2} = 10.15 K_{a3} = 8.1 K_{a4} = 6.41
Ferrous-Tan	Logk_1 =3.205	Logk_1=3.254

The Table shows the values of dissociation constant and stability constant for ligand and binary complexes and the effect of ionic strength, which were determined according to Irving Rossotti's

method. Figure 5 and Table 2 demonstrate how the protonation constants of Tan decrease in the presence of ionic strength, hence decreasing the degree of ligand dissociation, by looking at the dissociation and stability constants for ligand and binary complexes. Additionally, the stability constants of the metal ion in complexes with ligand are larger than those of the complexes without ionic strength, indicating a stronger ligands between the metal and Tan.

Effect of temperature

The effect of temperature on the binary complexes of Tan with iron ions was investigated with a constant concentration of 0.01 M and at different temperatures, where three temperatures were chosen (298.15K, 310.15K, and 313.15K) as shown in Figure 6, where iron-Tan complexes were formed at all temperatures due to convergence and spacing of the Tan curve and iron with Tan curve then convergence there again.

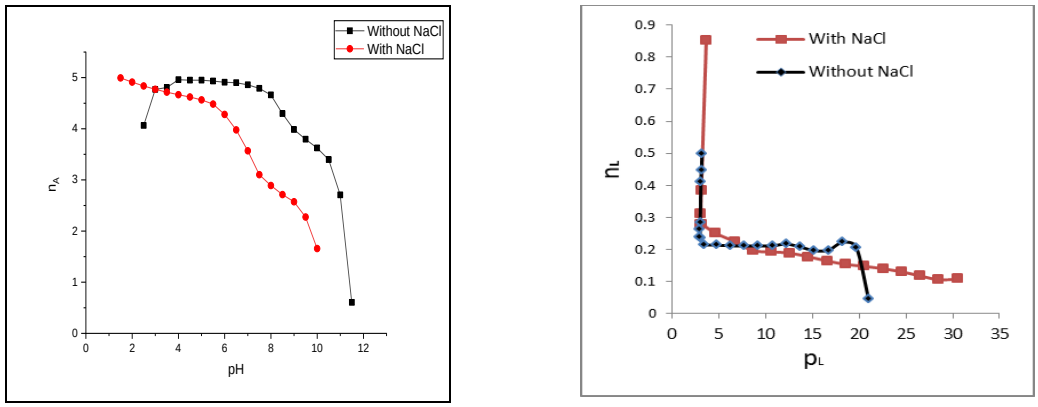

Figure 5: Potentiometric titration (A), and Protonation constant Curves (B) of ferrous-ASC, Glut, TA complexes at presence 0.1M NaCl, 310.15 K and 0.01M

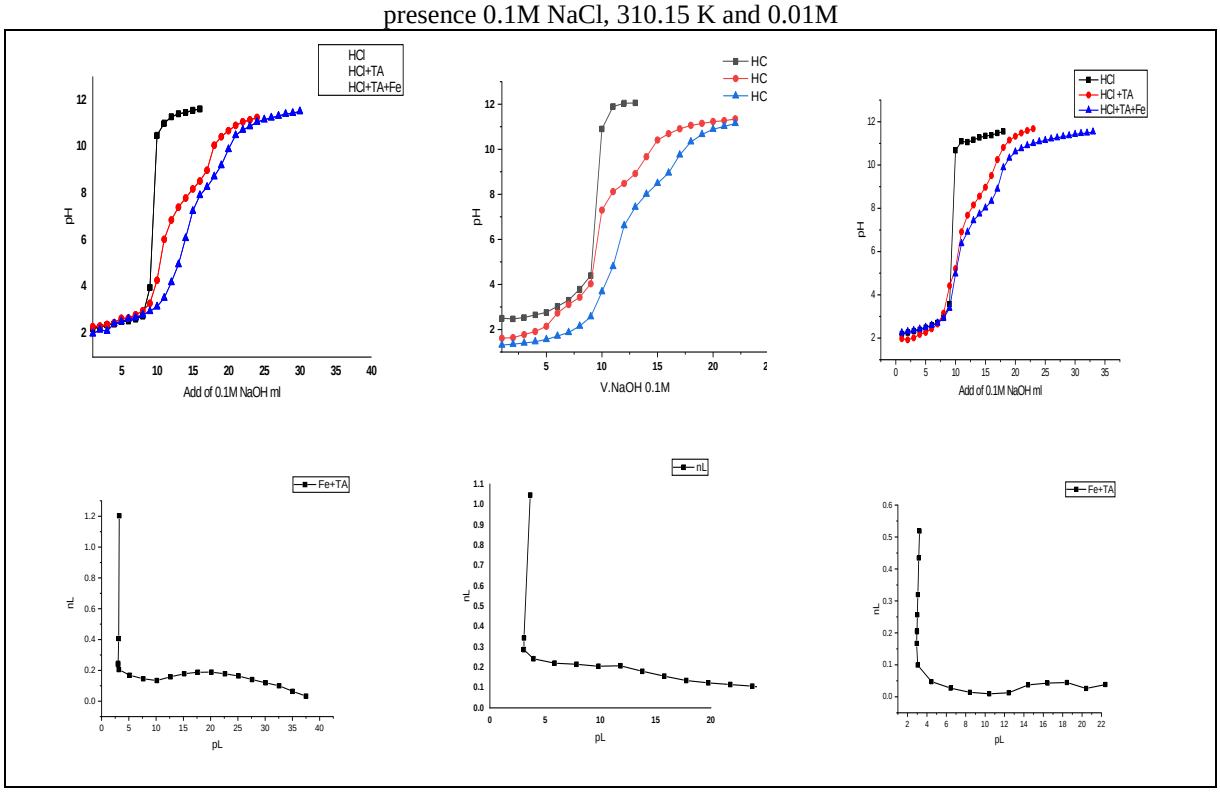

Figure (6). potentiometric titration and Formation constant curves of binary ferrous complexes at 298.15K,313.10K

Effect of temperature

The effect of temperature on the binary complexes of Tan with iron ions was investigated with a constant concentration of 0.01 M and at different temperatures, where three temperatures were chosen (298.15K, 310.15K, and 313.15K) as shown in Figure 6, where iron-Tan complexes were formed at all temperatures due to convergence and spacing of the Tan curve and iron with Tan curve then convergence there again.

Analyzing Figure 6 and Table 3, it can be observed that metal ions with Tan produce a particular type of metal–ligand complexes: 1:1, with the absence of complexity being 1: 2 and the pH being independent at varying temperatures, The formation constant values iron-Tan complexes tend to increase with temperature as a result of increased interference between the iron and Tan ions, leading to higher nL values.

Table (3). Formation constants of binary iron complexes at different temperature

Comp.	298.15 K	310.15 K	313.15 K
Tan	K_{a1}=11.65	K_{a1} =11.51	$K_{a1=}$ 12.5
	K_{a2} =11.08	K_{a2} =11.3	K_{a2} = 12. 0
	K_{a3} = 10.15	K_{a3} = 11.08	K_{a3}= 11.15
	K_{a4} = 8.05	K_{a4} = 10.35	K_{a4} = 9.1
	K_{a5} = 6	K_{a5} = 8.2	K_5= 7.0
	K_{a6}=/	K_{a6} = 2.4	K_6= 2.3
Iron-Tan	log K_1=3.156	log K_1=3.205	log K_1=3.215

Thermodynamic functions are the true measure of the interference strength between reactants and the nature of the studied system. This study was based on the results obtained from log K calculations at different temperatures, enthalpy values were calculated using the van't-Hoff relationship (Almutaleb & Alabbasi, 2023; Kemp, 1987).

$$logK = \frac{-\Delta H}{2.303RT} + \frac{\Delta S}{R} \qquad 8$$

By drawing the relation between log K and 1/T, a straight line with slope (-ΔH/2.303R) was given Figure 7, the interception was used to calculate the entropy (ΔS). Where R is the gas constant and T is the temperature.

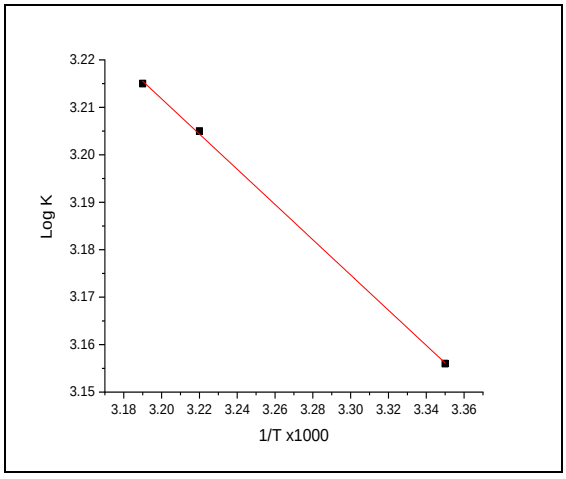

Figure(7). Application of Van't-Hoff relationship to iron - Tan complexes

Additionally the value of the change in free Gibbs energy (ΔG) was calculated through the relationship 9.

$$\Delta G = -2.303\ RT \log K] \qquad 9$$

The values of thermodynamic functions ΔS, ΔH, and ΔG for Tan with the metal ion complexes that were calculated are listed in Table 4.

Table (4). Values of thermodynamic functions of iron ion complexes at different temperatures and 0.01M

Thermodynamic functions		Values
R^2		0.9998
ΔH (KJ/mol)		+7.10741±0.0
ΔS (J/mol . k)		+36.57852±0.0
ΔG (KJ/mol)	298.15K	-18.01672
	310.15K	-19.03284
	313.15K	-19.27690

Table 4 shows the values of the thermodynamic functions of the binary iron complexes with the correlates under study. From this table, the following can be noted: I) The application of the Van't-Hoff equation gave a good linear relationship indicating that the value of the correlation coefficient is (0.999) for ferrous Tannic acid. II) A negative value of ΔG indicates that the reaction occurs spontaneously and its value decreases with the increase in temperature. III) ΔH values indicate that the reaction is endothermic. IV) positive ΔS values indicate that the interaction between ferrous and ligands is a random process

CONCLUSION

In this research, the stability constant (log K) and stoichiometric of these complexes were also investigated by the Potentiometric method, where the tannic acid binary complex only shows one formation constant at pH = 11.24 and log K = 3.205. The iron-Tan stoichiometric system indicates the formation of complexes was kept in the ratio 1:1. The Stability constants for all binary complexes increase with the increase of temperature; while they decrease in the presence of ionic strength the experimental data for thermodynamics indicates that the value of free energies (ΔG) of formation of the binary complexes becomes more negative with an increase in temperature. This shows that the complex formation is a spontaneous process and spontaneity increases with temperature, the enthalpy (ΔH) values indicate the endothermic nature of the complication reaction and explain the effect of temperature on the values of formation constants, and the entropy (ΔS) values indicate that the complex formation is (random process and randomized increases with temperature.

ACKNOWLEDGEMENT

We would like to thank the Chemistry Department of Sebha University for supporting us.

Duality of interest: The authors declare that they have no duality of interest associated with this manuscript.

Author contributions: Contribution is equal between authors.

Funding: No specific funding was received for this work.

REFERENCES

Abbaspour, N., Hurrell, R., & Kelishadi, R. (2014). Review on iron and its importance for human health. *Journal of research in medical sciences: the official journal of Isfahan University of Medical Sciences, 19*(2), 164.

Ahmad, T. (2014, 03/11). Reviewing the Tannic Acid Mediated Synthesis of Metal Nanoparticles. *Journal of Nanotechnology, 2014*, 1-11. https://doi.org/10.1155/2014/954206

Al-abbasi, A., Tahir, M., Kayed, S., & Kassim, M. (2022, 2022/04/01). Synthesis, characterisation and biological activities of mixed ligand oxovanadium (IV) complexes derived from N,N-diethyl-N′ -para-substituted-benzoylthiourea and hydrotris(3,5-dimethylpyrazolyl)borate [https://doi.org/10.1002/aoc.6607]. *Applied Organometallic Chemistry, 36*(4), e6607. https://doi.org/https://doi.org/10.1002/aoc.6607

Al-abbası A., B. N., Ahmida K., Zidan M. (2023). Potentiometric Studies on Binary and Ternary Complexes of Ni(II) and Cu(II) Ions with L-Valine and Paracetamol. *Journal of the Turkish Chemical Society Section A: Chemistry, 10*(2), 325-338. https://doi.org/https://doi.org/10.18596/jotcsa.1140039

Al-abbasi A., Z. M., Shnin N., Aldoori B. . (2023). Conductometric, Spectrophotometric and Computational Investigation of Binary and Ternary Complexes of Co(II) and Cu(II) Bivalent Metal Ions with L-Valine Amino Acid and Paracetamol Drug. *Journal of the Turkish Chemical Society Section A: Chemistry, 10*(3), 703-718.

Al-Saidi, H., Gouda, G., & Farghaly, O. (2020, 10/12). Potentiometric Study of a New Schiff Base and its Metal Ion Complexes: Preparation, Characterization and Biological Activity. *International Journal of Electrochemical Science*. https://doi.org/10.20964/2020.11.06

Almbrok, E. (2023, 10/17). Metal complexes and determination of nalidixic acid by potentiometric and conductometric methods.

Almutaleb, A. A. A., & Alabbasi, A. A. (2023). Synthesis, characterization and computational studies for (2′ S*,3R*,3′ S*,8a′ R*)-2′ ,3′ -bis(ethoxycarbonyl)-2-oxo-2′ ,3′ -dihydro-8a′ H-spiro[indoline-3,1′ -indolizine]-6′ -carboxylic acid and some derivatives. *Journal of Physical Organic Chemistry, 36*(2), e4452. https://doi.org/https://doi.org/10.1002/poc.4452

Baldwin, A., & Booth, B. W. (2022). Biomedical applications of tannic acid. *Journal of Biomaterials Applications, 36*, 1503 - 1523.

Belkher, N., Al-abbasi, A., and Zidan, M. . (2019). Potentiometric Studies on Stability Constant of the Complexes of SomeEssential Transition Metal Ions with L-Valine. *Journal of Pure & Applied Science 13*(3), 59-63.

Chen, X., Wang, Z., Wang, J., Yao, Y., Wang, Q., Huang, J., Xiang, X., Zhou, Y., Xue, Y., Li, Y., Gao, X., Wang, L., Chu, M., & Wang, Y. (2022). Role of tannic acid against SARS-cov-2 cell entry by targeting the interface region between S-protein-RBD and human ACE2. *Front Pharmacol, 13*, 940628. https://doi.org/10.3389/fphar.2022.940628

Cotoraci, C. A., Ciceu, A., Sasu, A., & Hermenean, A. O. (2021). Natural Antioxidants in Anemia Treatment. *International Journal of Molecular Sciences, 22*.

Dnkm, A., Al-Abbassi, A., & Erhayem, M. (2024, 2024/03/13). Synthesis and Characterization of Silver Nanoparticles Using Amberlite LA-2 Functionalized with Benzoyl Thiourea as a Capping Agent. *Chemistry Africa*. https://doi.org/10.1007/s42250-024-00902-9

Ems, T., & Huecker, M. R. (2019). Biochemistry, Iron Absorption.

Fu, Z., & Chen, R. (2019, 2019/02/03). Study of Complexes of Tannic Acid with Fe(III) and Fe(II). *Journal of Analytical Methods in Chemistry, 2019*, 3894571. https://doi.org/10.1155/2019/3894571

Hurrell, R., & Egli, I. (2010). Iron bioavailability and dietary reference values. *The American journal of clinical nutrition*, *91*(5), 1461S-1467S.

Irving, H. M., & Rossotti, H. S. (1954). The calculation of formation curves of metal complexes from pH titration curves in mixed solvents [10.1039/JR9540002904]. *Journal of the Chemical Society (Resumed)*, *638*(0), 2904-2910. https://doi.org/10.1039/jr9540002904

Irving, H. W., R. J. P. (1953). The stability of transition-metal complexes [10.1039/JR9530003192]. *Journal of the Chemical Society (Resumed)*, *637*(0), 3192-3210. https://doi.org/10.1039/jr9530003192

Kadiiska, M., Burkitt, M., Xiang, Q., & Mason, R. (1995). Iron supplementation generates hydroxyl radical in vivo. An ESR spin-trapping investigation. *The Journal of clinical investigation*, *96*(3), 1653-1657.

Kaufman, D. P., Kandle, P. F., Murray, I. V., & Dhamoon, A. S. (2024). Physiology, Oxyhemoglobin Dissociation Curve. In *StatPearls*. StatPearls Publishing, Copyright © 2024, StatPearls Publishing LLC.

Kemp, H. (1987). The effect of temperature and pressure on equilibria: a derivation of the van't Hoff rules. *Journal of Chemical Education*, *64*(6), 482.

Khalifa, S., AL-abbasi, A., Suliman, M. (2018). Adsorption and Corrosion Inhibition of Mild Steel in Acidic Media by Expired Pharmaceutical Drug. *Journal of Pure & Applied Sciences*, *17*, 1-6.

Maharani, F., Hartati, I., & Paramita, V. (2022, 12/29). Review on Tannic Acid: Potensial Sources, Isolation Methods, Aplication and Bibliometric Analysis. *Research In Chemical Engineering (RiCE)*, *1*, 46-52. https://doi.org/10.30595/rice.v1i2.33

McDermid, J. M., & Lönnerdal, B. (2012, 2012/07/01/). Iron. *Advances in Nutrition*, *3*(4), 532-533. https://doi.org/https://doi.org/10.3945/an.112.002261

McGee, E. J. T. (2017). *Prevention of Iron-Polyphenol Complex Formation in Iron Fortified Tea* University of Toronto (Canada)].

Moustarah, F., & Daley, S. F. (2024). Dietary Iron. In *StatPearls*. StatPearls Publishing Copyright © 2024, StatPearls Publishing LLC.

Piskin, E., Cianciosi, D., Gulec, S., Tomas, M., & Capanoglu, E. (2022, 2022/06/21). Iron Absorption: Factors, Limitations, and Improvement Methods. *ACS Omega*, *7*(24), 20441-20456. https://doi.org/10.1021/acsomega.2c01833

Suhud, K., Heng, L. Y., Rezayi, M., Al-abbasi, A. A., Hasbullah, S. A., Ahmad, M., & Kassim, M. B. (2015, 2015/02/01). Conductometric Studies of the Thermodynamics for Complexation of 1,1-Diethyl-3-(4-methoxybenzoyl)thiourea and Cobalt(II) Cation in Aqueous Binary Mixtures of Polar Organic Solvents. *Journal of Solution Chemistry*, *44*(2), 181-192. https://doi.org/10.1007/s10953-015-0308-2

Zheng, C., Shi, R., Jin, X., Qiu, Q., & Li, H. (2016, 2016/03/01/). Three complexes with helical frameworks based on l-glutamine and l-asparagine: Crystal structures and circular dichroism properties. *Inorganic Chemistry Communications*, *65*, 16-20. https://doi.org/https://doi.org/10.1016/j.inoche.2016.01.005

Al-Mukhtar Journal of Basic Sciences 22 (2): 134-140, 2024
Doi: https://doi.org/10.54172/2vgx1j05

Research Article

Open Access

Detection *Staphylococcus Aureus* Contaminated Some Door Handles and Table Surfaces and Their Sensitive to Antibiotics

Wafa A.Triki[1], Hosnia A. Boufarwa [2] and Nagah S. A. Abubaker [*]

***Corresponding author:** nagah.abubaker@omu.edu.ly, Department of Botany, Faculty of Science, Omar Al-Mukhtar University, Libya.

[1] Department of Environment, Faculty of Resources, Omar Al-Mukhtar University, Libya.

[2] Department of Botany, Faculty of Science, Omar Al-Mukhtar University, Libya.

Received:
15 May 2024

Accepted:
27 August 2024

Publish online:
31 August 2024

Abstract

The current study's objective was to identify and isolate *Staphylococcus* spp. germs from a few of Omar Al-Mukhtar University's faculty laboratories. It is regarded as the first investigation carried out at Omar Al-Mukhtar University to assess the level of Staphylococcal bacterial contamination of door handles and table surfaces inside the laboratories. 33 isolates from the College of Science's Botany Department were used in the study, which took place in the department's laboratories during the fall semester of the academic year (2022). After evaluating the expanding colonies and using morphological inspections and biochemical tests to diagnose the isolates, it was showen that 90.9% of the samples from the Botany Department were *Staphylococcus* and that the percentage of *S. aureus* reached 36.7% of isolates of *Staphylococcus*. A biofilm-forming capacity was demonstrated by 80% of the isolated bacteria, of which 29% were *S. aureus*. In order to ascertain the effectiveness of the antibiotics and which ones the bacteria are resistant to, the sensitivity of thirty *S. aureus* isolates to hospital-grade antibiotics against infection was tested. The findings revealed a high level of resistance to the majority of antibiotics and a definite resistance to gentamicin. Methicillin-resistant MRSA isolates made up 73.3% of the isolates, whereas vancomycin-resistant VRSA isolates made up 70%.

Keywords: Contamination ; table's surfaces ; door handles ; laboratories; *S.aureus*

INTRODUCTION

Every ecosystem is largely composed of microorganisms (Morris & Blackwood, 2024). [h1] In an academic setting, service desks are frequently accessible to visitors, staff, and students for a variety of reasons. Door handles have a very high risk of cross-contamination with bacteria since they are not regularly cleaned. Many people use the doors frequently, which lead to the collection of viruses, which, while entering and leaving, they pick up from somewhere else and put on the handles (Aiello et al., 2004). According to a study conducted in (Ayuba et al., 2019). to isolate and identify bacteria from staff office door handles in a few departments of the College of Science at Gombe State University, the traffic, exposure, and environment play important roles in changing the levels of contamination. The departments with the highest bacterial counts were those that contained These offices are used by a sizable number of department employees and students. According to (Otto, 2014), staphylococcus has been discovered on human body surfaces as part of the regular microflora and on environmental surfaces such as classroom door handles, toilets, tissues, the

bloodstream, and the noses of pets like cats and dogs. It has been documented that nearly every staphylococcal species can lead to opportunistic infections (Otto, 2009). Hazardous and potentially fatal infections such as severe sepsis, pneumonia, toxic shock syndrome, and endocarditis can be brought on by Staphylococcus aureus (Lowy, 1998). Staphylococci are harmful because they can enter the body and release a variety of endotoxins and blood enzymes (Todar, 2004). Biofilms developed which aid in the bacterial adhesion and colonization process (Forrest & Tamura, 2010). Furthermore, it was thought to be one of the most significant disease-causing variables that promote Staphylococcus attachment and colonization of tissues, which results in persistent infections since pathogens are difficult to eradicate (Darwish & Asfour, 2013). Every surface has microorganisms on it, and there are numerous direct and indirect ways for them to get there. According to the findings of the study carried out by (Umeanaeto et al., 2021), there was bacterial growth in 60.9% of the samples, with Staphylococcus spp. accounting for the largest number of isolated bacteria (20.5%).

The aim of research

To isolate and diagnose *Staphylococcus aureus* which contaminates door handles and table surfaces from some labs in the botany department at the Faculty of Science, And Screening of bacteria resistance to antibiotic and their capacity to form biofilm.

MATERIALS AND METHODS

Collecting of Samples and Bacterial Isolate Diagnosis

Samples were collected in 2022/2023 during the autumn season by swabs from the surfaces and placed on a selective media of mannitol salt agar (MSA) and were incubated at 37C° for 24-48 hours. The bacteria were purified for Identification. And then the bacteria suspicious grown colonies were based on Gram staining and standard biochemical reactions; including catalase, coagulase, and antibiotic susceptibility test (Habib et al., 2015; JF & Williams, 2000).

Detection of biofilm formation

To detect biofilm formation at a wavelength of 492 nm using a plate reader in accordance with (Shukla & Rao, 2017), measurements of the bacterial biofilm composition of some isolates are made using a microtitre plate; readings are obtained via a dish reader device (Erba Lisa Scan), and the OD is measured.

Screening of *Staphylococcus* species resistance to antibiotic

Nine antibiotics—Clindamycin, Oxacillin, Ampicillin, Tetracycline, Gentamicin, Trimethoprim, Doxycycline, Vancomycin, and Amoxicillin—were used in a sensitivity test on thirty isolates. According to the Clinical Laboratory Standards Institute (Wayne, 2011), the antibiotics were obtained from the Turkish business Bioanalyse in order to assess the susceptibility of *Staphylococci* Kirby-Bauer, 2016 and to explain the inhibition of diameter area using the disk diffusion method.

RESULTS

Identification of *S. aureus* isolates from research laboratories' door handles and table surfaces based on their morphological, biochemical, and biofilm-forming properties

In order to collect and identify bacteria found on table surfaces and handles in the labs of the Botany Department, College of Science, Omar Al-Mukhtar University, this study was carried out in the autumn semester of the academic year 2022. Following their isolation from laboratory table surfaces and handles, 33 isolates were identified based on their morphological and biochemical features, as listed in Table (1).

According to the findings, the majority of the isolates (30) were *Staphylococcus* bacteria, with 11 out of 30 being *S. aureus*. These findings were based on the morphological features of the colony on mannitol salt agar medium and Gram stain, as well as the catalase test and plasma coagulase enzyme test. Of these, 36.7% of the isolates were *S. aureus* coagulase in plasma and 63.3% were *Staphylococcus* negative.

Table (1) *Staphylococcus* and *S. aureus* isolates isolated from table surfaces and door handles in study laboratories according to morphological and biochemical characteristics and biofilm formation

Isolates	Colony color	Mannitol use	Gram stain	Cell shape	Catalase test	Coagulase test	Definition	biofilm formation
1	white	-	-	Spherical in chains	-	-	It is not *Staphylococcus*	+
2	white	-	-	Spherical in chains	-	-	It is not *Staphylococcus*	+
3	yellow	+	+	Spherical	+	+	S.aureus	+
4	Creamy	+	-	Spherical	-	+	Staph.	+
5	yellow	+	+	Spherical	+	+	S.aureus	+
6	white	+	-	Spherical	-	+	Staph.	+
7	white	+	-	Spherical	-	+	Staph.	+
8	yellow	+	+	Spherical	+	+	S.aureus	+
9	yellow	+	+	Spherical	+	+	S.aureus	+
10	white	+	-	Spherical	-	+	Staph.	+
11	yellow	+	+	Spherical	+	+	S.aureus	++
12	white	+	-	Spherical	-	+	Staph.	+
13	white	+	-	Spherical	-	+	Staph.	+
14	Creamy	+	-	Spherical	-	+	Staph.	+
15	Creamy	+	-	Spherical	-	+	Staph.	+
16	yellow	+	+	Spherical	+	+	S.aureus	-
17	Creamy	+	-	Spherical	-	+	Staph.	-
18	Creamy	+	-	Spherical	-	+	Staph.	-
19	Creamy	+	-	Spherical	-	+	Staph.	+
20	white	+	-	Spherical	-	+	Staph.	++
21	white	+	-	Spherical	-	+	Staph.	++
22	white	-	-	Spherical in chains	-	-	It is not defined	+
23	white	+	-	Spherical	-	+	Staph.	+
24	white	+	-	Spherical	-	+	Staph.	+
25	yellow	+	+	Spherical	+	+	S.aureus	+
26	white	+	-	Spherical	-	+	Staph.	++
27	yellow	+	+	Spherical	+	+	S.aureus	++
28	white	+	-	Spherical	-	+	Staph.	+
29	white	+	-	Spherical	-	+	Staph.	+
30	white	+	-	Spherical	-	+	Staph.	+
31	yellow	+	+	Spherical	+	+	S.aureus	-
32	yellow	+	+	Spherical	+	+	S.aureus	-
33	yellow	+	+	Spherical	+	+	S. aureus	-

+ Poor biofilm formation ++ Moderate biofilm formation -- No biofilm formation

Staphylococcus spp. screening for antibiotic resistance

Assessing the antibiotic sensitivity of *S.* aureus (Clindamycin, Oxacillin, Ampicillin, Tetracycline, Gentamicin, Trimethoprim, Doxycycline, Vancomycin, Amoxicillin) are the nine antibiotics that were used. In hospitals and clinics, these antibiotics are thought to be the most frequently utilized for treating bacterial infections. The results of the antibiotic sensitivity tests and the percentage of antibiotic resistance of the bacterial isolates are displayed in Table (2). The percentage of antibiotic

resistance varies from 0% to 100% for each isolate. The findings show that isolates No. 5,6,10,12,13, and 15 were sensitive to all tested antibiotics, while isolates No. 9,19,21, and 22 showed strong resistance at a rate of 88.9% and were susceptible to all tested antibiotics. Isolates No. 3,8,16,17,18,23, and 30 exhibited complete resistance to the antibiotics at a rate of 100%. Each of the isolates No. 2, 24, and 27 has a resistance rate of 77.8%, while the resistance rates of the remaining isolates range from 55.6% to 66.7%. The percentage of resistance and sensitivity of the *S. aureus* isolates tested to each antibiotic is displayed in Table (3). The results show that the antibiotic with the highest resistance percentage was Gentamicin, and the antibiotics with the lowest resistance percentage were Tetracyclin, Doxycycline, and Amoxicillin. The antibiotics with the highest resistance rates were Trimethoprim (76.7%) and Oxacillin (73.33%), where the resistance to Oxacillin is used as an indicator of MRSA bacteria.

Table (2). Susceptibility of *Staphylococcus sp.* and *Staphylococcus aureus* isolates and their resistance to antibiotics

Isolates	OX-10	AX-10	TE-10	VA-10	DO-30	CN-10	AM-10	SXT-25	CLN-30	Percentage of resistance of a single isolate to antibiotics
1	R	S	R	S	R	S	R	R	S	55.6%
2	S	R	R	S	R	R	R	R	R	77.8%
3	R	R	R	R	R	R	R	R	R	100%
4	S	S	S	S	R	R	R	R	R	55.6%
5	R	S	S	S	S	S	S	S	S	11.11%
6	R	S	S	S	S	S	S	S	R	22.2%
7	R	R	R	R	R	S	S	S	R	66.7%
8	R	R	R	R	R	R	R	R	R	100%
9	R	R	R	R	R	R	R	R	S	88.9%
10	R	S	S	S	R	R	S	S	S	33.3%
11	S	R	R	R	R	S	R	S	R	66.7%
12	S	R	S	S	R	S	R	S	S	33.3%
13	R	S	S	R	S	S	S	R	R	44.4%
14	S	R	R	R	R	S	R	S	S	55.6%
15	S	S	S	S	S	S	S	S	S	0
16	R	R	R	R	R	R	R	R	R	100%
17	R	R	R	R	R	R	R	R	R	100%
18	R	R	R	R	R	R	R	R	R	100%
19	R	R	R	R	R	R	S	R	R	88.9%
20	S	S	R	S	R	R	R	R	S	55.6%
21	R	R	R	R	R	S	R	R	R	88.9%
22	R	R	R	R	R	R	S	R	R	88.9%
23	R	R	R	R	R	R	R	R	R	100%
24	R	R	R	R	R	R	R	S	S	77.8%
25	R	S	R	R	R	R	R	S	S	66.7%
26	R	S	R	R	R	S	S	S	R	55.6%
27	R	R	R	R	R	S	R	S	R	77.8%
28	S	R	R	S	R	R	R	R	S	66.7%
29	R	R	R	R	R	R	R	R	S	88.9%
30	R	R	R	R	R	R	R	R	R	100%

S is sensitive to antibiotics **R** is resistant to antibiotics

Table (3). Percentage of sensitivity and resistance of *Staphylococcus aureus* isolates to antibiotics

Antibiotic	Sensitivity	resistance%
Clindamycin	33.33%	66.67%
Oxacillin	26.67%	MRSA 73.33%
Ampicillin	33.33%	66.67%
Tetracyclin	40%	60%
Gentamicin	13.33%	86.67%
Trimethoprim	23.33%	76.67%
Doxycycline	40%	60%
Vancomycin	30%	70%
Amoxicillin	40%	60%

DISCUSSION

According to a study, the microscopic diagnosis of Gram-stained slides revealed that the cells were spherical, clustered, and positive for Gram stain. In (Chakraborty et al., 2011) All isolates had the capacity to withstand a high concentration of mannitol salt, according to the results of biochemical tests, which is in line with a study's findings (Ahmed et al., 2010) and that the mannitol sugar can be fermented by *S. aureus*. The discoloration of the medium to a yellow hue distinguishes the strain in question from certain staphylococci strains that lack the capacity to metabolize mannitol, thus preserving the medium's original coloration. Furthermore, empirical evidence from biochemical analyses has confirmed that each staphylococcal isolate exhibits catalase enzyme activity, a trait corroborated by the results of the plasma coagulation enzyme test, which relies on this enzymatic activity. Specifically, Staphylococcus aureus, as the producer of coagulase enzyme, contrasts with other Staphylococci species that do not produce the enzyme essential for plasma coagulation. These discernible distinctions align with the conventional characterization of staphylococcal bacteria. (Baron et al., 1994; JF & Williams, 2000). 80% of the *Staphylococcus* isolates, according to the results of the biofilm formation test, were able to form biofilm. Of these, 29% were isolated from the *S. aureus* species, of which 20.8% had a high ability to form biofilm and 79.1% had a moderate ability. The outcomes supported the researcher's conclusions (Erfani et al., 2015): Our study's findings were consistent with the researcher's, since 80% of *staphylococcal* isolates develop biofilm (Tsopmene et al., 2023) All isolates of *Staphylococcus* spp. produced biofilms; 12.69% produced strong biofilms, 77.77% produced moderate biofilms, 9.52% produced weak biofilms, and so on.

The percentage of resistance for Vancomycin was 70% and the lowest percentage was 66.7% for both Clindamycin and Ampicillin. The results of our research agreed with the researcher's findings (Yeh et al., 2011). The majority of *Staphylococcus* spp. isolates are resistant to Ampicillin, which contradicts the findings of the researcher (Noel et al., 2017) who found that Gentamicin is the antibiotic with the lowest resistance rate, 15.3%, for the majority of *Staphylococcus* spp. isolates. Additionally, the results of the researcher (Domínguez et al., 2002) showed that the isolates of *Staphylococcus* had low resistance to Clindamycin, Gentamicin, Tetracycline, and Oxacillin, with resistance rates of 2.6%, 13%, 20.5%, and 25.6%, respectively, and high sensitivity against Vancomycin. Furthermore, the results of our study converged with the researcher (Vaez et al., 2011), as the isolates demonstrated high resistance to Ampicillin, and our findings where the *Staphylococcus* isolates did not accord with the researcher's findings about the isolates' susceptibility to vancomycin and gentamicin at 100% and 76%, respectively, and demonstrated resistance to amoxicillin, oxyacillin, telacyclin, and clindamycin. The results obtained by the researcher mentioned did not align with our findings (Nazarchuk et al., 2020). Sensitivity to gentamicin in S. aureus was noted at 42.86%, whereas sensitivity to doxycycline stood at 65.38%. Our study's results were consistent with those reported in Shaker's investigation from 2018, revealing that Staphylococcus isolates showcased resistance to a spectrum of antibiotics, including Amoxicillin, Gentamicin, Vancomycin, Ampicillin, Oxacillin, and Trimethoprim.

CONCLUSION

The study's findings indicate that *Staphylococcus* species, including *S. aureus*, were widely distributed on laboratory door and table handles. It demonstrated that *Staphylococci* were treated with antibiotics in hospitals and clinics despite their various resistance. The implementation of treatment recommendations and the establishment of a robust national action plan to address antibiotic resistance are crucial for countries, as contaminated hands can spread bacteria to handles and table surfaces within university buildings. Numerous isolates that are resistant to various antibiotics oc-

cur as a result of the use of multiple antibiotic kinds. Because overusing antibiotics can lead to a number of issues, including the emergence of new strains of antibiotic-resistant bacteria and the development of antibacterial resistance, we advise only using antibiotics when absolutely necessary and in the appropriate manner. Be cautious to prevent infection by often washing your hands and avoiding close contact with ill persons. Door handles play a significant part in the transfer and spread of bacteria and should therefore be given special attention during sterilization since the transmission of bacteria from stainless steel surfaces to the hands is increased.

Duality of interest: The authors declare that they have no duality of interest associated with this manuscript.

Author contributions: Contribution is equal between authors.

Funding: No specific funding was received for this work.

REFERENCES

Ahmed, M. O., Abuzweda, A. R., Alghazali, M. H., Elramalli, A. K., Amri, S. G., Aghila, E. S., & Abouzeed, Y. M. J. L. J. o. M. (2010). Misidentification of methicillinresistant Staphylococcus aureus (MRSA) in hospitals in Tripoli, Libya. *5*(1).

Aiello, A. E., Marshall, B., Levy, S. B., Della-Latta, P., Larson, E. J. A. a., & chemotherapy. (2004). Relationship between triclosan and susceptibilities of bacteria isolated from hands in the community. *48*(8), 2973-2979.

Ayuba, L., Suwange, M., Enefiok, U. J. I. J. o. M. S., & Technology. (2019). Bacterial contamination of door handles/knobs in gombe state university, Nigeria. *4*(8), 204-211.

Baron, E. J., Peterson, L., & Fenigold, S. (1994). Diagnostic Micobiology.(9th edn.) Mosby Publication. In: USA.

Chakraborty, S. P., KarMahapatra, S., Bal, M., & Roy, S. J. A. A. J. M. S. (2011). Isolation and identification of vancomycin resistant Staphylococcus aureus from post operative pus sample. *4*(2), 152-168.

Darwish, S. F., & Asfour, H. A. J. T. S. W. J. (2013). Investigation of biofilm forming ability in Staphylococci causing bovine mastitis using phenotypic and genotypic assays. *2013*(1), 378492.

Domínguez, E., Zarazaga, M., & Torres, C. J. J. o. c. m. (2002). Antibiotic resistance in Staphylococcus isolates obtained from fecal samples of healthy children. *40*(7), 2638-2641.

Erfani, M., Ghasemi, D., Mirnejad, R., & Piranfar, V. (2015). Incidence and antibiotic susceptibility pattern of Staphylococcus spp. in urinary tract infections (UTI), Iran, 2013-2014.

Forrest, G. N., & Tamura, K. J. C. m. r. (2010). Rifampin combination therapy for nonmycobacterial infections. *23*(1), 14-34.

Habib, F., Rind, R., Durani, N., Bhutto, A. L., Buriro, R. S., Tunio, A.,…Sciences, B. (2015). Morphological and cultural characterization of Staphylococcus aureus isolated from different animal species. *5*(2), 15-26.

JF, M. J. L., Williams, & Williams, B. (2000). Biochemical tests for identification of medical bacteria.

Lowy, F. D. J. N. E. j. o. m. (1998). Staphylococcus aureus infections. *339*(8), 520-532.

Morris, S. J., & Blackwood, C. B. (2024). The ecology of soil biota and their function. In *Soil microbiology, ecology and biochemistry* (pp. 275-302). Elsevier.

Nazarchuk, O. A., Nahaichuk, V. I., Osadchuk, N. I., Dmytriiev, D. V., Dmytriiev, K. D., & Turzhanska, O. S. J. W. L. (2020). Prognostic parameters of the susceptibility of Staphylococcus spp. to aminoglycosides and doxycycline. *73*(8), 1615-1619.

Noel, C. d. C., Silvério, F. M., Francisco, N. L. d. S. G., Almeida, N. R. d., & Soares, L. d. C. J. R. b. c. s. (2017). Suscetibilidade antimicrobiana e fatores de virulência de Staphylococcus em fômites do hospital universitário sul fluminense. 245-254.

Otto, M. J. C. o. i. m. (2014). Staphylococcus aureus toxins. *17*, 32-37.

Otto, M. J. N. r. m. (2009). Staphylococcus epidermidis—the'accidental'pathogen. *7*(8), 555-567.

Shukla, S. K., & Rao, T. S. J. B. (2017). An improved crystal violet assay for biofilm quantification in 96-well microtitre plate. 100214.

Todar, K. G. (2004). *Todar's online textbook of bacteriology*. Kenneth Todar University of Wisconsin-Madison Department of Bacteriology.

Tsopmene, U. J., Iwewe, Y. S., Eyong, I. M., Bisso, B. N., & Dzoyem, J. P. J. C. (2023). Antibiotic Resistance Profile, Biofilm Formation Ability, and Virulence Factors Analysis of Three Staphylococcus spp. Isolates From Urine. *15*(4).

Umeanaeto, P. U., Okafor, U. C., Unam, M. C., Ilo, C. C., Okoli, C. C., Afulukwe, S. C.,…Sciences, L. (2021). Assessment of parasites and bacterial contamination of office door handles in nnamdi azikiwe university, Awka, Anambra State. *9*(2), 120-127.

Vaez, H., Tabaraei, A., Moradi, A., & Ghaemi, E. A. J. A. J. M. R. (2011). Evaluation of methicillin resistance Staphylococcus aureus isolated from patients in Golestan province-north of Iran. *5*(4), 432-436.

Wayne, P. (2011). Clinical and laboratory standards institute. Performance standards for antimicrobial susceptibility testing.

Yeh, P. J., Simon, D. M., Millar, J. A., Alexander, H. F., Franklin, D. J. O. p. h., & perspectives, r. (2011). A diversity of Antibiotic-resistant Staphylococcus spp. in a Public Transportation System. *2*(3), 202-209.

Al-Mukhtar Journal of Basic Sciences 22 (2): 141-147, 2024
Doi: https://doi.org/10.54172/ncp5k696

Research Article

Open Access

A preliminary recording of insects on the island of Farwa Northwest of Libya

Hoda M. Elmareme[1], Abdulhamed M. Etriieki[2*], Asmaa D. Mkhebesh[3], Ali A. Bataw[4], Munay A. Albarbar[5], Nahad S. Ben Omar[6]

Corresponding author: abdulhamed.etriieki@gu.edu.ly, Department of Zoology, Faculty of Science, University of Gharyan, Gharyan, Libya

[1] Department of Zoology, Faculty of Science, University of Tripoli, Tripoli, Libya.

[3] Department of Ecology, Faculty of Science, Sabratha University, Sabratha, Libya

[4] Department of Zoology, Faculty of Science, University of Omar Al Mukhtar, Al-Bayda, Libya

[5] Department of Zoology, Faculty of Science, University of Tripoli, Tripoli, Libya.

[6] Department of Zoology, Faculty of Science, University of Tripoli, Tripoli, Libya.

Received:
28 June 2024

Accepted:
30 August 2024

Publish online:
31 August 2024

Abstract

The study aimed to present the first record of insect families in Farwa Island. Farwa Island is the largest and most important island in Libya; located in Northern west part of Libya in the Mediterranean, its insect fauna is poorly studied. Short time intensive collection of insect samples was conducted in four areas (mouth of the valley, bay of containers, center of the Island, and Ras-Attalgha) in February, March and April 2021. Different methods were used for insect collection, sorting, preservation and later identification to the lowest taxonomic level and verification. 9 orders, 31 families, 40 genera and 58 insect species were collected in the study; the center of the Island had the highest numerical density and diversity of insect fauna due to its diverse vegetation compared to other areas. Diverse suitable habitats and absent insect control measures provided suitable environmental conditions for insects breeding, feeding and hiding from enemies. This study constitutes the first comprehensive survey of insect fauna on Farwa Island and adds significant value to the ongoing assessment of insect diversity in Libya. A long-term study has to be conducted to investigate detailed information about the abundance and diversity of insects and other arthropods on Farwa Island.

Keywords: Collection, Biodiversity, Farwa Island, Insect fauna, Libya

INTRODUCTION

Insects are invertebrate animals (Phylum: arthropods) that comprise the largest known and most widely distributed group (Class: Insecta) of multicellular organisms worldwide. Although the estimates of their numbers may vary, most entomologists agree that there are approximately 1.1 million described insect species. However, estimates of their actual number vary from 1.5 to 5 million species, and a consensus is converging on about 3.5 million species (roughly three times the number of described species) (Grimaldi, 2023). Insects are found in almost all environments, on plants, around

buildings and under objects such as rocks and tree trunks; aquatic insects can be found in lakes, ponds, streams, rivers and swamps. Many insects have direct or indirect impacts on humans (pests as those considered parasitic, disease-transmitting vectors or homes/agricultural products destroying organisms). Moreover, insects are considered the most ecologically significant land organisms based on their large biomass. Some insect species are very destructive to forests and crops, but they constitute only a small percentage, and their numbers are biologically controlled by parasitoids and predatory insects. About 80-85% of the world's flowering plants are pollinated by insects; some insect products (honey, silk, dyes, wax and sustainable protein) are indispensable materials for humans. The fruit fly *Drosophila melanogaster* (as an experimental organism) has inspired the scientific society with many significant discoveries and breakthroughs in biology and other related fields (Grimaldi and Engel, 2005; Mohamed and Shaurub, 2010; Grimaldi, 2023).

Farwa Island is the biggest and most significant Island in Libya. It is situated 150 km west of Tripoli in the Northwest part of Libya on the Mediterranean Sea at the border region between Libya and Tunisia. The Island is roughly 12 km long with a maximum width of approximately 3 km, and the total surface area is about 31 km^2. Coordinates: 33°06'20.3"N 11°44'39.2"E. With its location in the Mediterranean climate zone, Farwa Island has a temperate climatic condition with sunny days and northern winds dominating most of the year. The mean annual temperature is 20ºC and the mean annual rainfall reaches 190 mm. The Island is characterized by a diverse collection of habitats (beaches, drying salt lakes, trees, sand dunes, marshes, mudflats and widespread tidal areas). These diverse environments provide a suitable habitat for many floral and faunal species (Etayeb, 2002; Etayeb and Essghaier, 2007; EGA-RAC/SPA, 2012; Isemmann *et al*., 2016).

Studies in Farwa Island on invertebrates groups generally and insect fauna particularly are poor. To the best of our knowledge, one previous study was conducted on invertebrates on this Island; the study by Jdeidi *et al.* (2015) revealed insects as the most abundant organisms (most of which were Coleoptera followed by Lepidoptera, Diptera, Hymenoptera and Orthoptera); it also included spiders and scorpions. This research introduces the first thorough study of recorded insect families in Farwa Island.

MATERIALS AND METHODS

The study was conducted during the months of February, March and April 2021. The Island was divided into four areas: mouth of the valley, bay of containers, center of the Island, and Ras-Attalgha. (Figure 1).

The following tools and equipment were used: tweezers, manual collection net, white cloths (2 x 3 meters), umbrella with a diameter of 1 meter, jars of different sizes, plastic/glass tubes and containers for collecting ground insects, magnifying glass, notebook for recording sample data (sample number, date of collection and place of sampling). Each area was visited where samples were collected using different collection methods from using forceps to methods of hitting and shaking branches of the bushes.

The samples were collected over two periods from 10 am to 1pm and from 2 pm to 5 pm, kept alive in jars or plastic/glass tubes, sorted and labeled in the field based on areas and deposited in the laboratory of the biology department, faculty of science, University of Tripoli. They were then killed using pieces of cotton filled with 75% ethanol in sealed jars/tubes, and then pinned in tightly sealed insect boxes for later identification and verification. Classification to the lowest possible taxonomic level was conducted at the University of Tripoli and laboratory of biology department, faculty of science, Omar Al-Mukhtar University (Al Bayda) using binocular microscope and special references (Zavattari, 1934; Borror *et al.,* 1981; Beccaloni *et al.,* 2005; Lamas, 2008; Massa, 2009;

Kirk-Spriggs and Sinclair, 2017). The data of each sample and the level of its classification were placed on special sample cards for the purpose of permanent preservation and reference when needed.

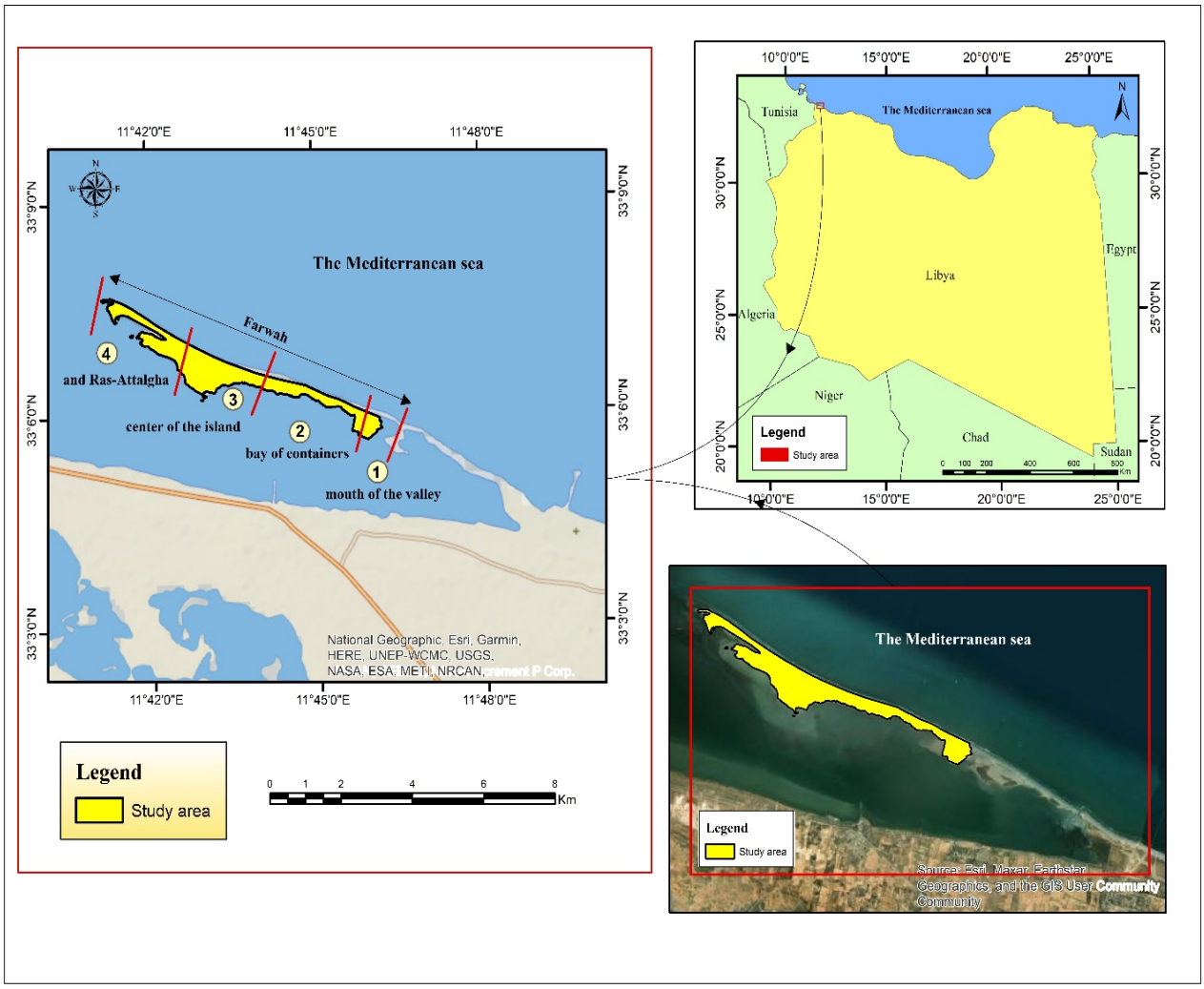

Figure: (1). Study area (Farwà Island) in the Northwest of Libya, divided into four regions: 1. mouth of the valley, 2. bay of containers, 3. center of the Island, and 4. Ras-Attalgha

RESULTS

The study collected 58 insect species belonging to 40 genera, 31 families and 9 orders, and they were arranged in (Table 1), followed by the scientific names for each insect. Four samples could be identified only to the family level (Asilidae, Reduvidae, Silphidae and Tetrigidae).

Table:(1). Orders, families and the scientific names of the collected specimens.

Order	Family	Scientific name
Coleoptera Linnaeus 1758	Carabidae Latreille 1802	*Scarites terricola* Bonelli 1913
	Cetoniidae Leach 1815	*Lophyra flexuosa* Fabricius 1787 *Oxythyrea funesta* Poda 1761 *Oxythyrea pantherina* Gory and Percheron 1883
	Coccinellidae Latreille 1807	*Coccinella septempunctata* Linnaeus 1758 *Coccinella undecimpunctata* Linnaeus 1758
	Scarabaeidae Latreille 1807	*Oxythyrea tripolitana* Reitter 1891
	Silphidae Latreille 1806	
	Tenebrionidae Latreille 1807	*Blapistinus histricus* Casey 1890 *Erodius zophosoides* Allard 1865 *Erodius bicostatus* Solier 1934 *Gonocephalum perplexum* Lucas 1846 *Himatismus villosus* Haag-Rutenberg 1870 *Phaleria acuminata* Küster 1852 *Pimelia granulata* Solier 1836 *Pimelia obsoleta* Solier 1836 *Pimelia urticata* Klug 1830 *Tentyria latreillei* Solier 1835 *Tentyrina duplicata* Reitter 1900
Dermaptera De Geer 1773	Forficulidae Stephens 1829	*Forficula auricularia* Linnaeus 1758
Diptera Linnaeus 1758	Labiduridae De Geer 1773 Asilidae Loew 1848	*Euborellia annulipes* Lucas 1847
	Bombyliidae Latreille 1802	*Systoechus vulgaris* Loew 1863
	Calliphoridae Robinaeu-Desvoidy 1830	*Calliphora vicina* Robineau-Desvoidy 1830 *Lucilia caesar* Linnaeus 1758 *Lucilia sericata* Meigen 1826
	Muscidae Latreille 1802	*Musca domestica* Linnaeus 1758
	Sarcophagidae Linnaeus 1758	*Sarcophaga carnaria* Linnaeus 1758
	Syrphidae Latreille 1802	*Eristalis tenax* Linnaeus, 1758
Hemiptera Linnaeus 1758	Coreidae Leach 1815	*Anasa tristis* De Geer 1773
	Lygaeidae Schilling 1829	*Spilostethus pandurus* Scopoli 1763
	Pentatomidae Leach 1815	*Eurygaster hottentotta* Fabricius 1775
	Reduvidae Linnaeus 1758	
Hymenoptera Linnaeus 1758	Apidae Linnaeus 1758	*Xylocopa ruficeps* Friese 1910
	Formicidae Latreille 1809	*Cataglyphis bicolor* Fabricius 1793 *Cataglyphis nigra* André 1881 *Cataglyphis nodus* Brullé 1833 *Cataglyphis oasium* Menozzi 1932 *Cataglyphis viatica* Fabricius 1787 *Messor aegyptiacus* Emery 1878 *Messor arenarius* Fabricius 1787 *Messor barbarus* Linnaeus 1767 *Messor minor* André 1883
	Scoliidae Latreille 1802	*Scolia erythrocephala* Fabricius 1798

Order	Family	Scientific name
Lepidoptera Linnaeus 1758	Lycaenidae Leach 1815	*Aricia agestis* Denis and Schiffermüller 1775
	Noctuidae Latreille 1809	*Agrotis infusa* Boisduval 1832
	Pieridae Swainson, 1820	*Pieris brassicae* Linnaeus 1758
		Pieris rapae Linnaeus 1758
		Pontia daplidice Linnaeus 1758
	Pterophoridae Zeller 1841	*Gillmeria pallidactyla* Haworth 1811
	Zygaenidae Latreille 1809	*Zygaena felix* Oberthür 1876
Odonata Fabricius 1793	Libellulidae Rambur 1842	*Sympetrum decoloratum Selys 1884*
		Sympetrum fonscolombii Selys 1840
Orthoptera Latreille 1793	Acrididae MacLeay 1819	*Acrotylus insubricus* Scopoli 1786
		Oedipoda caerculescens Linnaeus 1758
		Oedipoda fuscocincta Lucas 1849
		Oedipoda miniata Pallas 1771
		Omocestus rufipes Zetterstedt 1821
		Truxalis nasuta Linnaeus 1758
	Gryllotalpidae Saussure 1870	*Neocurtilla hexadactyla* Perty 1832
	Tetrigidae Rambur 1838	
Thysanura Linnaeus 1758	Lepismatidae Linnaeus 1758	*Lepisma saccharina* Linnaeus 1758

DISCUSSION

Insects are indispensable organisms for life on earth and for the functioning and sustainability of all ecosystems (Saxena and Omkar, 2023). Based on a short-term intensive survey, this paper constitutes the first comprehensive collection of insects on Farwa Island. Moreover, in view of the importance of the study of insects in Libya in general and Farwa Island in particular, this study (represented by 9 orders, 31 families, 40 genera and 58 insect species) was compared to other similar studies; a study conducted by Yahiya (2014) included similar families (Coreidae, Lycaenidae, Lygaeidae, Pentatomidae, Pieridae). Similarly, a study by Mifsud (2000) had Carabidae, Coccinellidae, Formicidae, Sarcophagida and Tenebrionidae, and another study by EL-Meghrabi (2009) included Lygaeidae, Pentatomidae and Reduvidae, all of which were recorded in this survey. This study recorded the presence of families Zygaenidae, Noctuidae, Silphidae, Scoliidae, which were not present in the aforementioned studies (Yahiya, 2014), (Mifsud, 2000), (El-Meghrabi, 2009). 77 families obtained in the aforementioned studies were not recorded in this survey. This study was the first of its kind in the sampling and classification of insects on the Island, specifically among the areas and environments in which insects were collected and classified.

This insect biodiversity was due to the presence of many suitable habitats that may provide appropriate environments for both insects breeding and hiding from enemies. Moreover, the absence of control measures also helped to increase the abundance and distribution of insects in the study area

The results were obtained from samples collected only from Farwa Island and a multiplicity of insect habitats was observed, especially in the central region of the Island because of the diversity of vegetation compared to the number of visits to the study areas. On the other hand, the rest of the study areas, such as the mouth of the valley, and Ras-Attalgha, had the least numeri-

cal density and diversity of insect families due to the large number of waves and sea currents that result in strong winds for the two areas and thus the inappropriateness of climatic conditions, in addition to the scarcity of vegetation. The presence of insect families near plants was more abundant, followed by sand, and the least was near dung and carrion.

CONCLUSION

The results of this short time intensive survey of insects on Farwa Island showed that the Island has relatively abundant and diverse insect fauna. This is due to the fact that the Island provides suitable environments for insects breading, feeding and escaping enemies; the absence of insect control measures adds to this rich biodiversity. Based on this comprehensive collection of insects from Farwa Island, this research adds important value to the continuously growing evaluation of the insect fauna in Libya.

ACKNOWLEDGEMENT

Authors declare there is no acknowledgement. No financial assistance was received in support of the study.

ETHICS

This article is original. The authors declare no ethical issues that may arise after the publication of this manuscript.

Duality of interest: The authors declare that there is no duality of interest associated with this manuscript.

Author contributions: All the authors contributed equally to preparing, developing and carrying out this manuscript.

Funding: This work did not receive any funding (institutional, private or corporate financial support). The authors self-funded their study.

REFERENCES

Beccaloni G., Scoble M., Robinson G. & Pitkin, B. (2005) The Global Lepidoptera names index. Natural History Museum. Available from http://www.nhm.ac.uk/our-science/data/lepindex/index.html

Borror, D.J., De Long, D.M., Triplehorn, C.A., (1981). An Introduction to the Study of Insects, fifth ed. Saunders College Publishing

EGA-RAC/SPA Waterbird Census Team, (2012). Atlas of wintering water birds of Libya, 2005-2010. Imprimerie COTI, Tunisia.

El-Meghrabi, M. S. (2009). Survey of some Heteropterous insects in Libya. Journal of Productivity and Development, 14(3), 747-758.

Etayeb K.S., (2002). A study of Migratory and resident Marine Birds in Ras Attalgha and the Western part of Farwa island. M. Sc. Thesis. Tripoli University. Tripoli, Libya.

Etayeb K.S. & Essghaier M.F.A., (2007). Breeding of marine birds on Farwa Island, western Libya. *Ostrich*, 78(2), 419–421. http://dx.doi.org/10.2989/OSTRICH.78.2.48.128.

Grimaldi, D and Engel, M.S. (2005). *Evolution of the Insects*. Cambridge University Press, Cambridge, UK.

Grimaldi, D. A. (Ed.). (2023). *The Complete Insect: Anatomy, Physiology, Evolution, and Ecology*. Princeton University Press.

Isemmann P., Hering J., Brehme S., Essghaer M., Etayeb K.S., Bourass E. & Azafzaf H., (2016). Birds of Libya. Groupe Horizon, France, 302 pp.

Jdeidi, T. B., Saed, F. A., and Elhosk, M. A. (2015). *The Main Fauna and Flora of Farwa Island,* Libya.

Kirk-Spriggs, A.H. and Sinclair, B.J. (eds). (2017). Manual of Afrotropical Diptera. Volume 1. Introductory chapters and keys to Diptera families. Suricata 4. South African National Biodiversity Institute, Pretoria; pp. 267–355

Lamas, G. (2008). Global butterfly names: various checklists. Taxome Project. Available from http://www.ucl.ac.uk/taxome/gbn/

Linnaeus, C., (1758). Systema Naturae, sive regna tria naturae systematice proposita per classes, ordines, genera et species. Holmiae (Stockholm), 824pp.

Massa, B. (2009). Annotated check-list of Orthoptera of Libya. *Journal of Orthoptera Research*, 18(1), 75–93. http://dx.doi.org/10.1665/034.018.0109

Mifsud, D. (2000). Present knowledge of the entomofauna of the Maltese Islands. Entomologica Basiliensia 22: 75-86.

Mohamed, W.F and Shaurub, E.S.H. (2010). A checklist of some recorded insects in Misurata, Libya. *Journal of King Saud University (Science)*, 22(2), 61-65. doi:10.1016/j.jksus.2010.02.001

Saxena, S., Omkar (2023). Insects in Scientific Research Advancement. In: Omkar (eds) Insects as Service Providers. Springer, Singapore. https://doi.org/10.1007/978-981-19-3406-3_9

Yahiya, Y.M, (2014). Common insects of orders Coleoptera, Lepidoptera and Hemiptera in middle region of Al-Jabal Al-Khdar, Libya. *Middle East Journal of Agriculture Research,* 3(3), 395-397.

Zavattari, E. (1934). Prodromo della fauna della Libia. Tipografia già Cooperativa,Pavia, i-viii+1234pp

Al-Mukhtar Journal of Basic Sciences 22 (2): 148-158, 2024
Doi: https://doi.org/10.54172/v8ree613

Research Article **Open Access**

Some properties of *-weak rings with involution

Muna E. Abdulhafed[1*] and Aafaf E. Abduelhafid[2]

***Corresponding author:**
muna.am2016@gmail.com,
Department of Mathematics, Faculty of Science, University of Azzaytuna, Tarhunah, Libya.

[2] Department of Mathematics, Faculty of Education, University of Azzaytuna, Tarhunah, Libya.

Received:
08 July 2024

Accepted:
29 August 2024

Publish online:
31 August 2024

Abstract
Throughout this paper, we introduced the concept of *-weak (*-IFP, quasi-*-IFP, and *-reversible) *-rings also study properties and the basic structure of *-weak *-rings, giving some of the results. Moreover, we will clarify the conditions for the *-weak *rings to extend into subrings with the involution of the ring, at the upper triangular matrices $(T_{n\times n}(R)$, with the same diagonal).

Keywords: ***-weak *-IFP; ***-weak quasi *-IFP; ***-weak *-reversible *-rings.

INTRODUCTION

All the rings, in this case, are associated with R unity. Mapping $*: R \longrightarrow R$ is an involution if $(a+b)^* = a^* + b^*$, $(ab)^* = b^*a^*$ and $(a^*)^* = a$ for all $a, b \in R$. A *-ring R is called *-zero divisor, for any $a \neq 0$. If $ab = ba^* = 0$, for some $0 \neq b \in R$ since R is an integral domain of involution if there are no nonzero zero divisors with involution, see [(Usama A. Aburawash and Khadija B. Sola, 2010)]. A self-adjoint idempotent; $e^2 = e = e^*$, is called projection. A nonempty subset S of a *-ring R is called self-adjoint or *-subset if $S^* = \{s^* | s \in S\} = S$, and from (U. A. Aburawash & Saad, 2016), defined semi-proper involution $*$ (resp. proper) if $aRa^* \neq 0$ (resp. $aa^* \neq 0$) for $0 \neq a \in R$, If $a^n = 0 = (aa^*)^m$ for some $n, m \in \mathbb{Z}^+$, then a is called *-nilpotent *-ring. Moreover, a *-ring R is said to be *-reduced if it has no nonzero *-nilpotent elements, and a *-ring R is called *-Baer if the *-right annihilator of each nonempty subset $A \in R$ is a principal *-bi-ideal generated by a projection; that is $r^*(A) = eRe$. Following (I. Kaplansky, 1968), A *-ring R is called Baer *-ring if the right annihilator of every nonempty subset of R is a principal right ideal generated by a projection, every Baer *-ring is a *-Baer ring with involution. From (Kim & Lee, 2003), R is semi-commutative or has an IFP ring if for every $a, b \in R$, if $ab = 0$ implies $aRb = 0$ or ($r(a)$ is an ideal of R for any $a \in R$. In (U. A. Aburawash & Saad, 2014) and (U. A. Aburawash & Saad, 2019), a *-ring R is called IFP with involution (resp. quasi-IFP with involution) if $ab = 0$ (resp. $ab = 0 = ab^*$) implies $aRb^* = 0$ (resp.; $aRb = 0$), for all $a, b \in R$. According to (U. A. Aburawash & Saad, 2019), (U. A. Aburawash & Abdulhafed, 2018b), and (U. A. Aburawash & Abdulhafed, 2018a), if $ab = 0 = ab^*$ implies $ba = 0$ (resp.; ba is central) for all $a, b \in R$ is called *-reversible (resp.; central *-reversible) *-ring. Every *-reversible *-ring has quasi-IFP with involu-

tion, a *-ring R is called weak *-IFP (resp.; weak quasi-IFP with involution), if $ab = 0$ (resp., $ab = 0 = ab^*$ for all $a, b \in R$ implies aRb^* is nilpotent (resp., aRb is nilpotent), a *-ring R central quasi IFP with involution (resp., has quasi-IFP with involution), if for all $a, b \in R$, $ab = 0 = ab^*$ implies aRb is central (resp., $aRb = 0$). the ring R is called weakly *-reversible, if $ab = ab^* = 0$, for all $a, b, r \in R$ then $Rbra$ is nil ideal of R.

In this article, every *-IFP is *-weak *-IFP, quasi *-IFP is *-weak quasi *-IFP and *-reversible is *-weak *-reversible, we study some properties *-weak *-rings it above. Moreover, a *-ring R is *-weak (*-IFP, quasi*-IFP, and *-reversible) if and only if for any n, the upper triangular matrix equal diagonal $T_{n\times n}(R)$ is *-weak (*-IFP, quasi*-IFP and *-reversible) *-ring. Further, we studied the extension of localization and Laurent polynomial of *-weak *-rings above.

***-weak *-IFP *-ring.**

Here section, we introduce another generalization for *-IFP; namely *-weak *-IFP *-rings.

Definition1. The *-ring R is called *- weak *-IFP, if $ab = 0$ implies aRb^* is *- nilpotent, for any $a, b \in R$.

Every *-IFP is *- weak *-IFP, and *- weak *-IFP is weak *-IFP. But the discourse is true by conduction semi-proper or central *- reversible.

Proposition1. If R is a weak *-IFP *-ring and semi-proper involution $*$ then R is *- weak *-IFP.

Proof. Let $ab = 0$ for some $a, b \in R$., $(arb^*)R(arb^*)^* = arb^*RbRa^* = a(rb^*R)bRa^* \subseteq aRbRa^* = 0$, by semi-proper involution $*$. Thus, R is *- weak *-IFP.

Proposition 2. Let R be a weak *-IFP *-ring and central *-reversible. Then R is *- weak *-IFP.

Proof. Let $ab = 0$ for some $a, b \in R$. Also, $bab = 0$ and $(baRb^*)^2 = baRb^*baRb^* = Rb^*babaRb^* = 0$,
$(baRb^*)(baRb^*)^* = baRb^*bRa^*b^* = Rb^*babRa^*b^* = 0$ for $r \in R$, by central *-reversible. Therefore, R is *- weak *-IFP.
Moreover, each commutative *-ring is *-weak *-IFP. The proof is easy with the following result.

Proposition 3. The class *-ring of the *-weak IFP with involution is closed (using changeless involution) by constructing *- subrings under its direct sums.

Proposition 4. Suppose that R be a commutative *-ring, then $T_{n\times n}(R)$ is a weak *-IFP *-ring, with involution * define as;

$$\begin{pmatrix} a & a_{12} & a_{13} & \cdots & a_{1(n-1)} & a_{1n} \\ 0 & a & a_{23} & \cdots & a_{2(n-2)} & a_{2n} \\ 0 & 0 & a & \cdots & \cdots & a_{3n} \\ \vdots & \vdots & \vdots & \ddots & \vdots & \vdots \\ 0 & 0 & 0 & \cdots & \cdots & a_{n-1(n)} \\ 0 & 0 & 0 & \cdots & \cdots & a \end{pmatrix}^* = \begin{pmatrix} a & a_{(n-1)n} & a_{(n-2)n} & \cdots & a_{2n} & a_{1n} \\ 0 & a & a_{23} & \cdots & a_{2(n-2)} & a_{1(n-1)} \\ 0 & 0 & a & \cdots & \cdots & a_{1(n-2)} \\ \vdots & \vdots & \vdots & \ddots & \vdots & \vdots \\ 0 & 0 & 0 & \cdots & \cdots & a_{12} \\ 0 & 0 & 0 & \cdots & \cdots & a \end{pmatrix}$$

(i.e., fix the two diagonals (right and left) with interchange the symmetric elements.)

Proof. If $A=(a_{ij})$ and $B=(b_{ij})\in T_{n\times n}(R)$ with $ab=0=ab^*$, where $1\le i\le j\le n$, then $ab=0$. By hypothesis, R is *-weak *-IFP, there exists $k\in\mathbb{N}$ such that $(acb)^k=0$ for any $C=(c_{ij})\in T_{n\times n}(R)$, since a, b and, c are the diagonal elements of A, B and, C with respective. Hence, there exists $n,m\in\mathbb{N}$ such that $((ACB^*)^k)^n=0,(((ACB^*)(ACB^*)^*)^k)^m=0$. Therefore, $T_{n\times n}(R)$ is *-weak *-IFP.

Now, every *-ring having*-IFP is *- weak*-IFP. The converse is true with semi-proper involution $*$, and each *- weak*-IFP *-ring is weak*-IFP *- ring while the converse is not true, as shown in the following example.

Example1. The *-ring $T_{3\times3}(\mathbb{Z})$with the involution * given by: $\begin{pmatrix}a&b&c\\0&a&d\\0&0&a\end{pmatrix}^*=\begin{pmatrix}a&d&c\\0&a&b\\0&0&a\end{pmatrix}$ is *-weak *-IFP by Proposition 4. For $A=\begin{pmatrix}0&1&0\\0&0&0\\0&0&0\end{pmatrix}$ and $B=\begin{pmatrix}0&1&1\\0&0&0\\0&0&0\end{pmatrix}$, we have $AB=0$ and $ARB^*=\begin{pmatrix}0&0&a\\0&0&0\\0&0&0\end{pmatrix}\neq0,a\in\mathbb{Z}$, so $T_{3\times3}(\mathbb{Z})$ has not *-IFP.

There is a weak semi-commutative (IFP) *-ring which is not *-weak IFP with involution, see **[(U. A. Aburawash & Abdulhafed, 2018b)**, Example 9].
Next, by Proposition 4, the ring $T_{2\times2}(R)$ is *-weak *-IFP. Also, $\mathbb{M}_{2\times2}(R)$ with self- adjoint has not *-weak *-IFP, since $A=\begin{pmatrix}1&0\\0&0\end{pmatrix},B=\begin{pmatrix}0&0\\0&1\end{pmatrix}$, satisfy $AB=0$ while $ACB^*=\begin{pmatrix}1&0\\0&0\end{pmatrix}\begin{pmatrix}x&y\\0&z\end{pmatrix}\begin{pmatrix}1&0\\0&0\end{pmatrix}=\begin{pmatrix}x&0\\0&0\end{pmatrix}\neq0,\ \forall\, x,y,z\in R.$

Therefore, we note that by diagram in the class of *-rings.

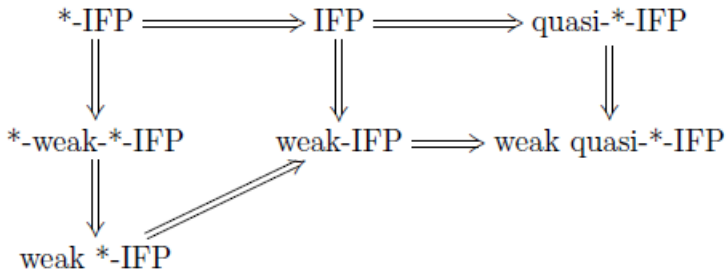

Diagram (1)

***- weak quasi *-IFP *-ring.**
In her section, we study the properties of the *-weak quasi-*-IFP rings with involution.

Definition 2. The *-ring R is called *- weak *-IFP, if for all $a,b\in R$, $ab=0=ab^*$ implies aRb is

*- nilpotent. Consequently, aRb^* is also *-nilpotent .Every commutative *-ring is *-weak quasi IFP with involution, each *-weak quasi-IFP with involution ring with involution is weak quasi-IFP with involution and *-weak quasi-IFP with involution ring with involution is quasi-IFP with involution, however, the converse is proper when the *-ring is semi-proper.

Proposition 5. Consider R is a weak quasi-*-IFP ring with involution and semi-proper involution $*$. Then R is the *- weak quasi-*-IFP *-ring.

Proof. Let $ab = 0 = ab^*$ for some $a, b \in R$, $(arb)R(arb)^* = arbRb^*Ra^* = a(rbR)b^*Ra^* \subseteq aRb^*Ra^* = 0$ for $a, b \in R$, by semi-proper involution $*$. Thus, R is *- weak *-IFP.

Proposition 6. Suppose that R is a central *-reversible *-ring and a weak quasi-IFP with involution. Then R is a *- weak quasi-IFP with involution.

Proof. If $ab = 0 = ab^*$ for some $a, b \in R$, then $bab = 0 = bab^*$ and $(baRb)^2 = baRbbaRb = baRbabRb = 0$,
$(baRb)(baRb)^* = baRbb^*Ra^*b^* = Rbbab^*Ra^*b^* = 0$, from central *-reversible. Thus, R is *-weak quasi-*-IFP.
Now, while there is no clear connection between *-weak quasi-*-IFP and weak- IFP. However, *-weak quasi-*-IFP R is weak- IFP if R has *-IFP.

Proposition 7. If R is *-weak quasi-*-IFP and R has IFP with involution, then R is a weak -IFP.

Proof. Since $ab = 0$ implies $aRb^* = 0$, by hypothesis and R is a weak IFP.

Further, the proposition below shows that *-subrings are the direct sums of the *-weak quasi-*-IFP *-ring.

Proposition 8. The class *-ring of the *-weak quasi-*-IFP is closed (using changeless involution) by constructing *- subrings under its direct sums.
Now, with the proof similar to Proposition 4, we get the following.

Proposition 9. It R is a commutative *-ring, $T_{n\times n}(R)$ is *-weak quasi-*-IFP, with involution * given in **Proposition 4.**
Next, is R is a commutative *-ring then

$$T_{n\times n}(R) = \left\{ \begin{pmatrix} a & a_{12} & a_{13} & \cdots & a_{1n} \\ 0 & a & a_{23} & \cdots & a_{2n} \\ 0 & 0 & a & \cdots & a_{3n} \\ \vdots & \vdots & \vdots & \ddots & \vdots \\ 0 & 0 & 0 & 0 & a \end{pmatrix} \middle| a, a_{ij} \in R, n \geq 3 \right\},$$

is *-weak quasi-*-IFP by **Proposition 9**. However, $T_{4\times4}(R)$ is not quasi-*-IFP, so in general in case $n \geq 4$ is not quasi-*-IFP.
Moreover, as an instance, we note that the condition $T_{n\times n}(R)$of Proposition 9, cannot be weakened to the whole matrix *-ring $\mathbb{M}_{n\times n}(R)$, because n is more than 1.

Example 2. Let R be the *-ring of integer numbers ($\mathbb{Z}$). Consider the *-ring is *- weak quasi-IFP with involution, while the *-ring $\mathbb{M}_{2\times2}(\mathbb{Z})$ with self-adjoint is not *-weak quasi-IFP with involution. For $A = \begin{pmatrix} 0 & 0 \\ 0 & a \end{pmatrix}$ and $B = \begin{pmatrix} 0 & -a \\ 0 & 0 \end{pmatrix}, a \in \mathbb{Z}$, satisfy $AB = 0 = AB^*$ and $C = \begin{pmatrix} 1 & 1 \\ 1 & 1 \end{pmatrix} \in \mathbb{M}_{2\times2}(R)$, thus $ACB = \begin{pmatrix} 0 & 0 \\ 0 & -a^2 \end{pmatrix}$ is not *-nilpotent.

Theorem1. Consider the following conditions, where R is a *-ring.

1. R is quasi-*-IFP.
2. R is central quasi-*-IFP.
3. R is *-weak quasi-*-IFP.
4. R is weak quasi-*-IFP.

Proof. $1 \Longrightarrow 2$: Obvious.
$2 \Longrightarrow 3$: : If $a,b \in R$ satisfied $ab = 0 = ab^*$, then arb, a^2rb, arb^2 and a^2rb^2 are central. Thus, $(arb)^2 = arbarb = a(arb)rb = r(a^2rb)b = ra^2rb^2 = ra(arb)b = r(arb)ab = 0$ and $((arb)(arb)^*)^2 = (arb)b^*r^*a^*(arb)b^*r^*a^* = b^*r^*a^*(arb)(arb)b^*r^*a^* = b^*r^*a^*(aarbrb)b^*r^*a^* = b^*r^*a^*(a^2rbrb)b^*r^*a^* = b^*r^*a^*(ra^2rb^2)b^*r^*a^* = b^*r^*a^*r(a(arb)b)b^*r^*a^* = b^*r^*a^*r((arb)ab)b^*r^*a^* = 0$
. Hence, arb is *-nilpotent for all $r \in R$ and R is *-weak quasi-*-IFP.
$3 \Longrightarrow 4$: It's clear.
Moreover, the discussion of Theorem 1 is invalidated by [(U. A. Aburawash & Abdulhafed, 2018a), Proposition 1] and Propositions (5 and 6).
The outcome can be obtained from [(U. A. Aburawash & Abdulhafed, 2018a), Proposition 1]and Theorem 1.

Corollary 1. Let R be *-ring and central quasi-IFP with involution, if R is a Baer ring with involution, then R is *-weak quasi-IFP with involution.

We know, every quasi-IFP with involution is *-weak quasi-IFP with involution, and by [(M. S. and U. A. Aburawash, 2023), propositions (4.2 and 5.1) and theorem 5.6)] the conclusion is obtained.

Corollary 2. Let R be a ring with involution and I a proper ideal a with involution of R. If I is a reduced with involution ring with involution (without identity) and R/I has quasi-IFP with involution, then R is also *-weak quasi-IFP with involution.

Corollary 3. Let R be a reduced with involution, ring with involution, and I an ideal with involution of R with IFP (as a ring without identity). If R has quasi-IFP with involution, then the *-subring S of the upper triangular matrix ring $T_{3\times3}(R)$ over R is defined as follows:

$$S = \left\{ \begin{pmatrix} a & d & c \\ 0 & a & b \\ 0 & 0 & a \end{pmatrix} \middle| a,b,c,d \in I \right\}, \text{ is *-weak quasi-*-IFP}$$

Corollary 4. Let R be a *-reduced *-ring and n any positive integer. If R is *-weak quasi-$*$-IFP, then $R[x]/\langle x^n \rangle$ is *-weak quasi-$*$-IFP.
Thus, we note that by a diagram, of *-rings.

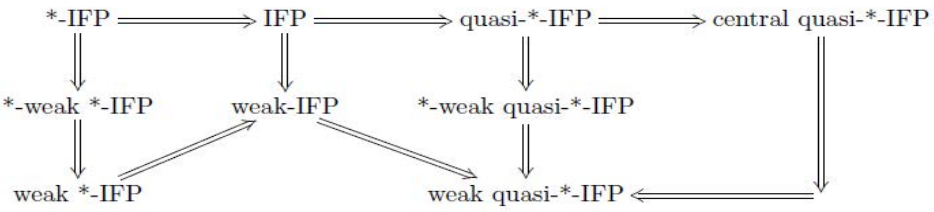

Diagram (2)

***- weak *-reversible *-ring.**
Here section, we introduce another generalization for *-reversible; namely *-weakly *-reversible *-rings.

Definition 3: A *-ring R is called *-weak *-reversible if for all $a,b,r \in R$, $ab = 0 = ab^*$, implies $Rbra$ is a *-nil left (equivalently, $braR$ is a *-nil right) *-ideal of R. Consequently, Rb^*ra is a *-nil left (equivalently, b^*raR is a *-nil right) *-ideal of R.

The commutative *-ring is *-weak *-reversible and each *-weak *-reversible *-ring is weak *-reversible. The converse is true while the *- ring has *-IFP as proven inside the following.

Proposition 10: If R *- ring has *-IFP and *-weak *-reversible, then R is weakly reversible**.**
Now, each *-weak *-reversible *-ring is weak *-reversible. The converse is true while the *- ring has semi-proper involution $*$ and central *-reflexive, we have the subsequent proposition.

Proposition 11: If R *-ring has semi-proper involution $*$ and weak *-reversible, then R is *-weak *-reversible.

Proof. Let $ab = 0 = ab^*$ for some $a,b \in R$. Then, $(Rbra)R(Rbra)^* = Rbra(Ra^*r^*)b^*R \subseteq RbraRb^*R = 0$, for all $r \in R$, from semi-proper involution $*$. Hence, R is *-weak *-reversible.

Recall that, [(U. A. Aburawash & Saad, 2019) and (U. A. Aburawash & Abdulhafed, 2018a)], if $ab = ab^* = 0$ implies $bRa = 0$ (resp., bRa is central) for all $a,b \in R$ is called *-reflexive (resp., central *-reflexive) *-ring. Every *-reversible is *-reflexive ring with involution.

Proposition 12: If R is weak *-reversible and central *-reflexive, then R is *-weak *-reversible since R is a *-ring.

Proof. Let $ab = 0 = ab^*$ for some $a,b \in R$. Then $(Rbra)^2 = RbraRbra = RRbrabra = 0$, $(Rbra)(Rbra)^* = Rbraa^*r^*b^*R = Ra^*r^*brab^*R = 0$, for all $r \in R$, from central *-reflexive. Hence, R is *- weak *-reversible.
Now, prove the next result it is easy.

Proposition 13. The *-weak *-reversible ring with involution class is closed under taking subrings with involution and under direct sums (with changeless involution).

Now, the next proposition is similar to **Proposition 4.**

Proposition 14. R is a commutative *-ring, $T_{n\times n}(R)$ is *- weak *-reversible, with involution * from **Proposition 4.**

In example 6 of **(U. A. Aburawash & Abdulhafed, 2018b)** there exists a *-weak *-reversible and quasi *-IFP *-ring which is not *-reversible.

Next, for example, we note that the condition $T_{n\times n}(R)$ of Proposition 14, cannot be weakened to the whole matrix *-ring $\mathbb{M}_{n\times n}(R)$, since n is more than 1.

Example 3. If R is a *-weak *-reversible *-ring and n is more than 1, then $\mathbb{M}_{2\times2}(R)$, with adjoint involution, is not *-weak *-reversible. For $X=\begin{pmatrix}0 & 1\\ 0 & 1\end{pmatrix}$ and $Y=\begin{pmatrix}0 & 1\\ 0 & 0\end{pmatrix}$, we have $XY=0=XY^*$ and for $Z=\begin{pmatrix}1 & 1\\ 0 & 1\end{pmatrix}\in\mathbb{M}_{2\times2}(R)$, we see that $RYZX=\begin{pmatrix}0 & 2a\\ 0 & 2c\end{pmatrix}$ is not *-nil, $\forall\, a,c\in R$.

The subsequent result shows that central *-reversible*-rings lie properly between *-reversible and *-weak*-reversible rings with involution.

Theorem 2. Consider the following conditions, where R is a *-ring.

1. R is *-reversible.
2. R is central *-reversible.
3. R is *-weak *-reversible.
4. R is weak *-reversible.

Proof. $1\Longrightarrow 2$: It's clear.
$2\Longrightarrow 3$: If $ab=0=ab^*$, then $r_1ab=0=r_1ab^*$ for all $a,b,r_1\in R$, and br_1a is central, since R is central *-reversible. Hence, $(rbr_1a)^2=rbr_1arbr_1a=rrbr_1abr_1a=0$ and $(rbr_1a)(rbr_1a)^*=rbr_1aa^*r_1{}^*b^*r^*=ra^*r_1{}^*br_1ab^*r^*=0$ for all $r\in R$ and R is weak *-reversible.
$3\Longrightarrow 4$: It's clear.
By [(U. A. Aburawash & Abdulhafed, 2018b), Propositions 3, 4] and Propositions (11 and 12) the converse of Theorem 2 isn't true.
Further, we get corollaries from [(U. A. Aburawash & Abdulhafed, 2018b), Proposition 4] and Theorem 2.

Corollary 5. Every *-domain is a *-weak *-reversible*-ring.

Corollary 6. If R is a central *-reversible and *-Baer ring with involution, then R is *-weak *-reversible.
It's important to remember that every Bear *-ring is a *-Bear *-ring. We have the following result.

Corollary 7. If R is a Baer and central *-reversible *-ring, then R is *-weak *-reversible.
Now, as shown by the next theorem, the central *-reversible*-rings properly lie between the classes of *-reversible, weak quasi-*-IFP, and *-weak quasi-*-IFP*-rings

Theorem 3. Consider the following conditions, where R is a *-ring.

1. R is *-reversible.
2. R is central *-reversible.
3. R is weak quasi-*-IFP.
4. R is *-weak quasi-*-IFP.

Proof. $1\Longrightarrow 2$: Obviously.

$2\Longrightarrow 3$: By [(U. A. Aburawash & Abdulhafed, 2018b), **Theorem 2**].
$3\Longrightarrow 4$: From Propositions (5 and 6).
The converse of **Theorem 3** is not true from [(U. A. Aburawash & Abdulhafed, 2018b), **Example 6**].

The following results, from [(U. A. Aburawash & Saad, 2019), **Proposition 10**], [(U. A. Aburawash & Abdulhafed, 2018b), **Corollaries** (**7, 8, 9, 10**)], and **Theorem 2.**

Corollary 8. If R is *-ring and central reduced then $T(R;R)$ is a *-weak *-reversible.

Corollary 9. If the *-ring R is reduced then $T(R;R)$ is a *-weak *-reversible.

Corollary 10. If the *-ring R is *-reduced and *-reversible, then $T(R;R)$, with componentwise involution, is *-weak *-reversible.

Corollary 11. If the *-ring R is reduced and *-reversible, then $T(R;R)$, with component wise involution, is *-weak *-reversible.
Thus, we note that by the diagram, of *-rings.

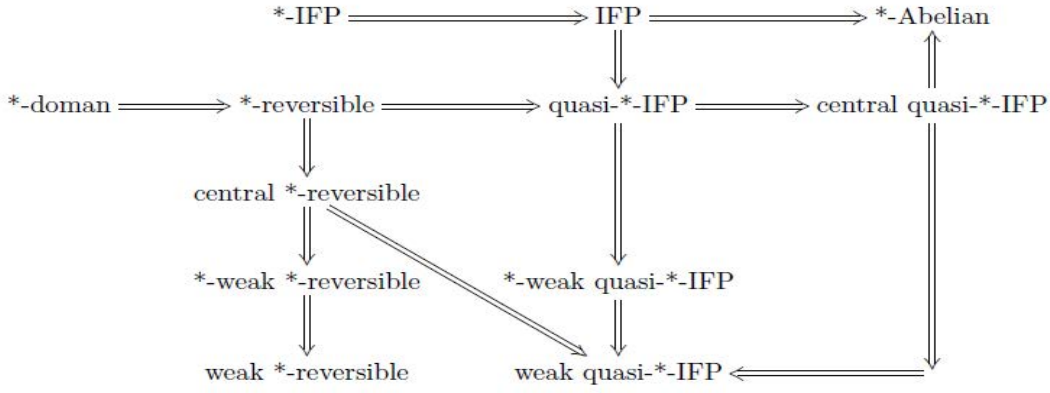

Diagram (3)

Extending of *-weak (*-IFP, quasi *-IFP, and *-reversible) rings with involution.

We will here focus on the properties of *-weak (*-IFP, the quasi –IFP with involution, and *-reversible) rings with involution is proven to be extended from a *-ring to its localization and Laurent polynomial, the Dorroh extension, and from Ore *-ring to its classical quotient.

If $\Omega^{-1}R = \{u^{-1}a \mid u \in \Omega, a \in R\}$, then $\Omega^{-1}R$ is a *-ring with involution $\circ$ defined as $(u^{-1}a)^{\circ} = u^{-1*}a^{*} = u^{*-1}a^{*}$ where R is a ring with involution, Ω is a multiplicative in R consisting of R and central regular elements, see **[(U. A. Aburawash & Abdulhafed, 2018b)].**
For it, we have the propositions.

Proposition 15. If e is a central projection of R since R is a *-ring, then it's equivalent.

1. R is *-weak quasi-*-IFP.
2. eR and $(1-e)R$ are *-weak quasi-*-IFP.
3. $\Omega^{-1}R$ is *-weak quasi-*-IFP.

Proof. $1 \Leftrightarrow 2$: It is clear that this is straightforward since subrings with involution and finite direct products of *-weak quasi-*-IFP ring with involution is *-weak quasi-*-IFP.
$3 \Longrightarrow 1$: It is clear since R is a subring with involution of $\Omega^{-1}R$.

$1 \Longrightarrow 3$: Since R is a *-subring of $\Omega^{-1}R$. Let $\alpha\beta = 0 = \alpha\beta^{\circ}$with $\alpha = u^{-1}a, \beta = v^{-1}b, u, v \in \Omega$ and $a, \mathrm{b} \in \mathrm{R}$, and let $\gamma = w^{-1}c$ for any element of $\Omega^{-1}R, w \in \Omega, \mathrm{c} \in \mathrm{R}$. Since Ω contained in the center of R, we have $0 = \alpha\beta = u^{-1}av^{-1}b = (u^{-1}v^{-1})ab$, and $0 = \alpha\beta^{\circ} = u^{-1}a(v^{-1}b)^{\circ} = (u^{-1}(v^{-1})^{*})ab^{*}$, and hence ab=0=ab^*, but R *-weak quasi-*-IFP, like this for some n and m in positive integers that $(\mathrm{acb})^{n} = 0, ((\mathrm{acb})(\mathrm{acb})^{*})^{m} = 0$. Thus $(\alpha\gamma\beta)^{n} = (u^{-1}aw^{-1}cv^{-1}b)^{n} = ((vwa)^{-1}acb)^{n} = ((vwa)^{-1})^{n}(acb)^{n} = 0$ and $((\alpha\gamma\beta)(\alpha\gamma\beta)^{\circ})^{n} = ((u^{-1}aw^{-1}cv^{-1}b)(\beta^{\circ}\gamma^{\circ}\alpha^{\circ}))^{n} = ((u^{-1}aw^{-1}cv^{-1}b)(\beta^{\circ}\gamma^{\circ}\alpha^{\circ}))^{m} = ((vwa)^{-1}(acb)(b^{*}(v^{-1})^{*}c^{*}(w^{-1})^{*}a^{*}(u^{-1})^{-1})^{m} = ((vwa)^{-1}(acb)(u^{*}w^{*}v^{*})^{-1}(b^{*}c^{*}a^{*}))^{m} = ((vwa)^{-1}(u^{*}w^{*}v^{*})^{-1}(acb)(b^{*}c^{*}a^{*}))^{m} = ((vwa)^{-1}(u^{*}w^{*}v^{*})^{-1})^{m}((acb)(acb)^{*}))^{m}$
. Therefore, $\Omega^{-1}R$ is *-weak quasi-*-IFP.

Proposition 16. If R is a *-ring, and e has a central projection in R, the following is its equivalent:

1. R is *-weak *-reversible.
2. eR and $(1-e)R$ are *-weak *-reversible.
3. $\Omega^{-1}R$ is *-weak *-reversible.

Proof. It is similar to that of **Proposition 15.**
We get results from**[(U. A. Aburawash & Abdulhafed, 2018b)**, Proposition 6].

Corollary 12. Let R be a *-ring, and e is a central projection of R. Then eR and $(1-e)R$ are *-reversible if R is *- weak *-reversible.

Corollary 13. If R is *-reversible a *-ring and e central of $e^{2} = e = e^{*}$in R. Then eR and $(1-e)R$ are *-weak *-reversible.

Then, the ring with involution of the Laurent polynomials in x, with coefficients in the *-ring R, consists of all formal sums $f(x) = \sum_{i=k}^{n} a_i x^i$ an involution *, $f^{*}(x) = \sum_{i=k}^{n} a_i^{*} x^i$ with explicit addition and multiplication, where $a_i \in R$ and k, n (possibly negative) integers. We denote this plate by $R[x; x^{-1}]$.

Corollary 14. For a *-ring R, Ω is *-weak quasi-*-IFP iff $R[x; x^{-1}]$ is *-weak quasi-IFP with involution.

Proof. It is sufficient to establish the necessity since $R[x]$ is a subring with involution of $R[x; x^{-1}]$. Let $\Omega = \{1, x, x^2, x^3, x^4, \cdots\}$. Then Ω is a multiplicative closed subset with the involution of Ω. Where $R[x; x^{-1}] = \Omega^{-1}R[x]$, it follows that $R[x; x^{-1}]$ is *-weak quasi-*-IFP by Proposition 15.

Corollary 15. For R *-ring, Ω is *-weak *-reversible if and if only $R[x; x^{-1}]$ is *-weak *-reversible.

Proof. Like **Corollary** 14 using Proposition 16.
Accordingly, we have the equivalence on *-weak quasi-*-IFP and *-weak *-reversibility of another situation.

Corollary 16. If R is a *-ring the following is its equivalent:

1) R is *-weak quasi-IFP with involution.
2) $R[x]$ is *-weak quasi-IFP with involution.
3) $R[x; x^{-1}]$ is *-weak quasi-IFP with involution.

Corollary 17. For a *-ring R, the following is its equivalent:

1. R is *-weak *-reversible.
2. $R[x]$ is *-weak *-reversible.
3. $R[x;x^{-1}]$ is *-weak *-reversible.

Then, for the Dorroh expansion of the *-ring $\mathrm{D}(\mathrm{R},\mathbb{Z}) = \{(\mathrm{r},\mathrm{n}): \mathrm{r} \in \mathrm{R}, \mathrm{n} \in \mathbb{Z}\}$ R is a ring whose functions are $(r_1,n_1)+(r_2,n_2) = (r_1+r_2, n_1+n_2)$ and $(r_1,n_1)(r_2,n_2) = (r_1r_2 + n_1r_2 + n_2r_1, n_1n_2)$. The R involution can naturally extend to $D(R,\mathbb{Z})$ in the form $(r,n)^* = (r^*,n)$ (see (U. A. Aburawash, 1997).

Next, we get the following results by [(U. A. Aburawash & Abdulhafed, 2018b), **Proposition 21**]:

Corollary 18. A *-ring R is *-reversible, and the Dorroh extension $D(R,\mathbb{Z})$ of R is *-weak-*-reversible.

Corollary 19. A *-ring R is Dorroh extension $D(R,\mathbb{Z})$ is *-reversible, R is *-weak-*-reversible.
We know that Let R be a ring with involution * which is a left order in a ring Q. Then R is a right order in Q and Q has an involution given by$(a^{-1}b)^* = b^*(a^*)^{-1}$ (see [(Martindale & 3rd, 1969), Lemma 4)], and [(U. A. Aburawash & Abdulhafed, 2018b), Theorem 4] given the following results.

Corollary 20. If R is *-reversible, then Q is *-weak-*-reversible.

Corollary 21. If Q is *-reversible, then R is *-weak-*-reversible.

CONCLUSION

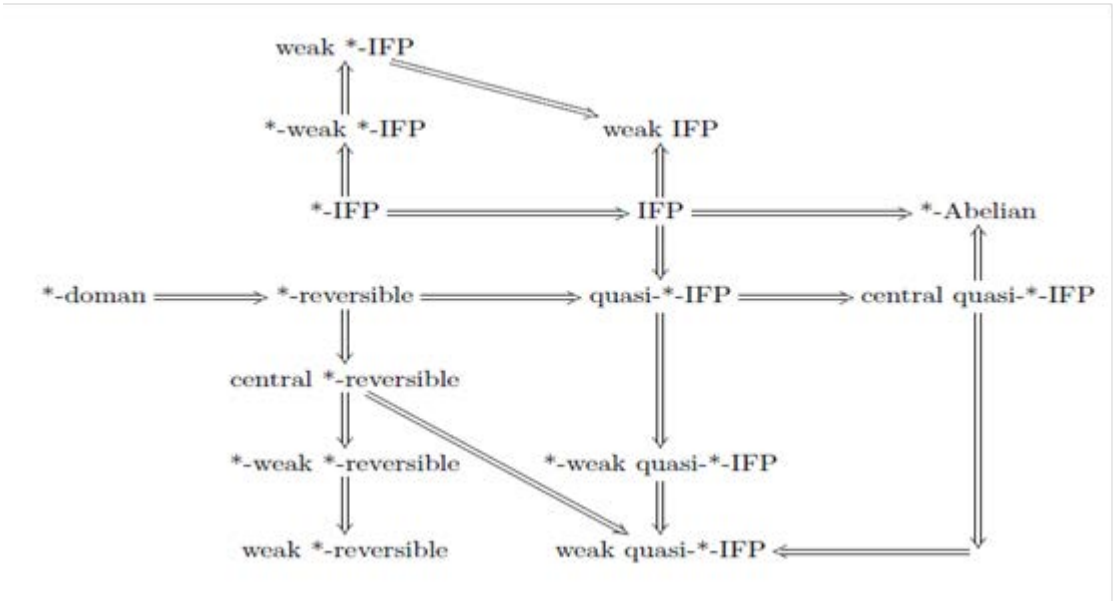

Here, we conclude the paper's results using diagrams to explain the relations among the corresponding classes, from diagrams [(1), (2)] and diagram (3).

Furthermore, we have the following conclusions:
Every *-IFP (resp., quasi *-IFP and *- reversible) are *-weak *-IFP (resp., *-weak quasi *-IFP and *-weak-*-reversible) rings with involution, also, each *-IFP is *-weak quasi *-IFP ring with involution. Moreover, every *-Doman is *-weak *-reversible ring with involution.

Finally, we future studies about properties of *-weak *- rings of (*-reflexive, S. *-reversible, and S. *-reflexive) rings with involution.

Duality of interest: The authors declare that they have a duality of interest associated with this manuscript.

Author contributions: The first author (Muna E. Abdulhafed) developed the theoretical formalism, and performed the analytic calculations into the final version of the manuscript. The second author (Aafaf E. Abduelhafid) collected the data, performed the analytic calculations, and analyzed the data.

Funding: The authors declare that we have never received any funding for the work reported in our manuscript.

REFERENCES

Aburawash, M. S. and U. A. (2023). IFP for rings with involution. *Mathematica Pannonica New Series*, *1*, 172–137.

Aburawash, U. A. (1997). On Embedding of Involution Rings. *Mathematica Pannonica*, *8*(2), 245–250.

Aburawash, U. A., & Abdulhafed, M. E. (2018a). On reflexive rings with involution. *International Journal of Algebra*, *12*(3), 115–132. https://doi.org/10.12988/ija.2018.8412

Aburawash, U. A., & Abdulhafed, M. E. (2018b). On reversibility of rings with involution. *East-West J. of Mathematics*, *20*(1), 19–36. https://doi.org/10.2140/pjm.1975.60.131

Aburawash, U. A., & Saad, M. (2014). On Biregular , IFP and Quasi-Baer *-Rings. *East-West J. of Mathematics Mathematics*, *16*(2), 182–192.

Aburawash, U. A., & Saad, M. (2016). *-Baer property for rings with involution. *Studia Scientiarum Mathematicarum Hungarica*, *53*(2), 243–255. https://doi.org/10.1556/012.2016.53.2.1338

Aburawash, U. A., & Saad, M. (2019). Reversible and reflexive properties for rings with involution. *Miskolc Mathematical Notes*, *20*(2), 635–650. https://doi.org/10.18514/MMN.2019.2676

I. Kaplansky. (1968). *Rings of Operators*. Benjamin, New York.

Kim, N. K., & Lee, Y. (2003). Extensions of reversible rings. *Journal of Pure and Applied Algebra*, *185*(1–3), 207–223. https://doi.org/10.1016/S0022-4049(03)00109-9

Martindale, W. S., & 3rd. (1969). Rings with involution and polynomial identities. *Journal, of Algebra*, *11*, 186–194.

Usama A. Aburawash and Khadija B. Sola. (2010). *-zero divisors and *-prime ideals. *East-West J. of Mathematics*, *12*, 27–31.